

Pontryagin Differentiable Programming: An End-to-End Learning and Control Framework

Wanxin Jin Purdue University wanxinjin@gmail.com
Zhaoran Wang Northwestern University zhaoranwang@gmail.com
Zhuoran Yang Princeton University zy6@princeton.edu
Shaoshuai Mou Purdue University mous@purdue.edu

Abstract

This paper develops a Pontryagin differentiable programming (PDP) methodology, which establishes a unified framework to solve a broad class of learning and control tasks. The PDP methodology distinguishes from existing methods by two novel techniques: first, we differentiate the Pontryagin’s Maximum Principle, and this allows us to obtain analytical gradient of a trajectory with respect to a tunable parameter of a system, thus enabling end-to-end learning of system dynamics, policy, or/and control objective function; and second, we propose an auxiliary control system in backward pass of the PDP framework, and show that the output of the auxiliary control system is exactly the gradient of the system trajectory with respect to the parameter, which can be iteratively obtained using control tools. We investigate three learning modes of the PDP: inverse reinforcement learning, system identification, and control/planning, respectively. We demonstrate the capability of the PDP in each learning mode using various high-dimensional systems, including multilink robot arm, 6-DoF maneuvering UAV, and 6-DoF rocket powered landing.

1 Introduction

Many learning tasks can find their counterpart problems in control fields. These tasks seek to obtain unknown aspects of a system with different terminologies used by both fields compared below.

Table 1: Topic correspondence between control and learning (details presented in Section 2)

UNKNOWN IN A SYSTEM	LEARNING METHODS	CONTROL METHODS
Dynamics $\mathbf{x}_{t+1} = \mathbf{f}_{\theta}(\mathbf{x}_t, \mathbf{u}_t)$	Training Neural Network	System Identification
Policy $\mathbf{u}_t = \pi_{\theta}(\mathbf{x}_t, t)$	Reinforcement Learning (RL)	Optimal Control (OC)
Control Objective $J = \sum_t c_{\theta}(\mathbf{x}_t, \mathbf{u}_t)$	Inverse RL	Inverse OC

With the above task correspondence, learning and control communities have begun to explore the complementary benefits of the other: control theory may provide abundant models and structures that allow the algorithm to scale to high-dimensional tasks, while learning enables to obtain models from data, which are otherwise not readily attainable using classic control theory. Examples that enjoy the mutual benefits include model-based RL [1, 2], where dynamics is used to alleviate sample complexity; and Koopman-operator control [3, 4], where via learning, a nonlinear system is lifted to an observable space for which linearity still holds. Inspired by those examples, this paper aims to exploit the benefits of both areas and develop a unified framework to solve a range of learning and control problems, e.g., the challenging continuous-space tasks shown in Fig. 1.

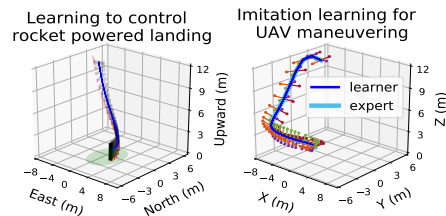


Figure 1: left: PDP to learn rocket landing control, right: PDP to learn UAV dynamics and control objective for imitation.

2 Backgrounds and Related Work

Learning dynamics. Control fields refer to it as system identification, and typically consider linear dynamics represented by transfer functions [5]. For non-linear systems, Koopman theory [6] can be used to lift a nonlinear system to observable space, where linearity still holds [3, 7, 8]. Identifying (lifted) linear dynamics is treated as least-square regression [9, 10]. In learning fields, recent work [11–18] studies (deep) neural networks as dynamics models, where the activation value of each layer and network parameter corresponding to state and parameter of the dynamical system, respectively. Thus, training a neural network becomes identifying a dynamics model. See [19] for a recent survey.

The proposed PDP method in this work can be used for learning dynamics models, but different from the above methods, it takes a *trajectory variation* perspective, and the key question in the learning process is to ask *how the trajectory of a system varies by a small change of its dynamics*. The PDP learns (nonlinear) dynamics model over trajectory spaces instead of lifting to observable spaces, and also the learning process is more explainable than training general-purpose neural networks.

Learning optimal policies. In learning fields, this relates to reinforcement learning (RL). Built on dynamic programming, model-free RL does not require analytical dynamics models, but evaluates and improves a policy by directly interacting with the environment/system. Although achieving significant success [20–22], but it usually suffers from high sample complexity (especially for continuous-space tasks). Model-based RL overcomes this by first learning a dynamics model, then integrating it to policy improvement [1, 23–25]. The counterpart topic in control fields is optimal control (OC). *OC however is more concerned with the existence and characterization of an optimal trajectory solution (open loop) in presence of dynamics models*. As in RL, the main strategy to solve OC is also dynamic programming, and many valued-based methods have been developed, such as solving HJB [26] (a PDE equation, which can be thought of as a differential version of Bellman equation for continuous cases), differential dynamical programming (DDP) [27], which uses second-order approximations of the dynamics model and value function, and iterative linear quadratic regulator (iLQR) [28], which uses first-order approximation of the dynamics and second-order approximation of the value function.

The second strategy to solve OC is use of the Pontryagin’s Maximum/Minimal Principle (PMP) [29]. Derived from calculus of variations, the PMP can be looked at as optimizing a control objective function over the space of trajectories of a control system (by solving a set of ODEs equations). Thus, the PMP avoids the necessity of characterizing or approximating value functions (i.e., avoiding solving PDEs of HJB). This is a fundamental difference from dynamic programming techniques such as valued-based OC and RL [27, 28]. Some available OC solvers use this idea of trajectory optimization, such as the single-shooting or multiple-shooting methods [30, 31], where the optimization variable is the entire or segments of the system trajectory with concatenation constraints.

The proposed PDP method in this paper can be used to solve optimal control problems. However, fundamentally different from any dynamic-programming based RL or OC methods (e.g., DDP and iLQR), the PDP method is derived from PMP and thus is essentially a *trajectory-variation* method. Specifically, it minimizes an objective (cost/reward) function through investigating the *analytical variation of the system trajectory with respect to the change of the policy*. This looks similar to the direct shooting methods [30] which also finds an optimal trajectory, but a slight difference is that the PDP solves OC by minimizing the objective over a parameterized policy instead of over trajectories.

Learning control objective functions. This relates to inverse reinforcement learning (IRL) in learning fields, whose goal is to find an underlying control objective (cost/reward) function to explain given demonstrations. The unknown objective function is typically parameterized as a weighted sum of features [32–34]. Strategies to learn the unknown weights include feature matching [32] (matching the feature values of demonstrations and predicted trajectories), maximum entropy [33] (finding a trajectory distribution of maximum entropy subject to empirical feature values), and maximum margin [34] (maximizing the margin of objective values between demonstrations and predicted trajectories). The counterpart problem in control is inverse optimal control (IOC) [35–38]. Based on the knowledge of dynamics, IOC focuses on more efficient learning paradigms. For example, by directly minimizing the violation of optimality conditions by observed data, [35, 38, 39] directly solve the feature weights without repetitively solving the corresponding OC problems.

The proposed PDP can also be used for IRL/IOC. A fundamental difference from existing IRL/IOC techniques is that the PDP *investigates the analytical variation/gradient of trajectory with respect to the control objective function*, and this allows us to minimize the loss between demonstrations and predicted trajectory *directly* with respect to the unknown control objective using gradient descent.

Comparison with Other Learning Frameworks. The difference and comparison of algorithm complexity between the proposed PDP and other learning frameworks are discussed in Appendix F.

Claim of Contributions. To the learning area, the proposed PDP is an *explainable* and *structural* method capable of efficiently solving high-dimensional continuous-space tasks: first, different from existing methods, the PDP *adopts a trajectory perspective for learning* and investigates the *analytical variation/gradient of a trajectory with respect to unknown parameter of a system*; and second, to that end, the PDP proposes the auxiliary control system in backward pass of learning process, and the *output of the auxiliary control system is exactly the variation/gradient of the trajectory with respect to the parameter*, which can be iteratively solved. To the control community, to our best knowledge, this is the first work to *develop the technique of variation/differentiation of the PMP*, and importantly, we *introduce the auxiliary control system and prove that differentiation of the PMP is equivalent to solving the auxiliary system*. These two techniques fundamentally differ from the linearization methods, e.g., DDP or iLQR, which are based on dynamical programming and linearize/quadratize dynamics/value functions with the variable directly being a trajectory.

3 Problem Statement

We begin with a general problem formulation and then discuss how to accommodate such formulation to specific applications. Consider a class of optimal control systems $\Sigma(\theta)$, which is parameterized by a tunable $\theta \in \mathbb{R}^r$ in both dynamics and control objective function:

$$\Sigma(\theta) : \begin{array}{ll} \text{dynamics:} & \mathbf{x}_{t+1} = \mathbf{f}(\mathbf{x}_t, \mathbf{u}_t, \theta) \quad \text{with given } \mathbf{x}_0, \\ \text{control objective:} & J(\theta) = \sum_{t=0}^{T-1} c_t(\mathbf{x}_t, \mathbf{u}_t, \theta) + h(\mathbf{x}_T, \theta). \end{array} \quad (1)$$

Here, $\mathbf{x}_t \in \mathbb{R}^n$ is the system state; $\mathbf{u}_t \in \mathbb{R}^m$ is the control input; $\mathbf{f} : \mathbb{R}^n \times \mathbb{R}^m \times \mathbb{R}^r \mapsto \mathbb{R}^n$ is the dynamics model, which is assumed to be twice-differentiable; $t = 0, 1, \dots, T$ is the time step with T being the time horizon; and $J(\theta)$ is the control objective function with $c_t : \mathbb{R}^n \times \mathbb{R}^m \times \mathbb{R}^r \mapsto \mathbb{R}$ and $h : \mathbb{R}^n \times \mathbb{R}^r \mapsto \mathbb{R}$ denoting the stage and final costs/rewards, respectively, both of which are twice-differentiable. For a choice of θ , the system $\Sigma(\theta)$ will produce a trajectory of state-inputs

$$\xi_\theta = \{\mathbf{x}_{0:T}^\theta, \mathbf{u}_{0:T-1}^\theta\}, \quad (2)$$

which optimizes the control objective function $J(\theta)$ while subject to the dynamics \mathbf{f} . For many applications (we will show next), one evaluates the above trajectory ξ_θ using a scalar-valued differentiable loss $L(\xi_\theta, \theta)$. Then, the **problem of interest** is to tune the system parameter θ , such that the system trajectory ξ_θ has the minimal loss, that is, one wants to solve

$$\min_{\theta} L(\xi_\theta, \theta) \quad \text{s.t.} \quad \xi_\theta \text{ is generated by } \Sigma(\theta). \quad (3)$$

In the above problem formulation, we think of $\Sigma(\theta)$ as a **configurable box**. For a specific learning or control task, we can accordingly change the setting of $\Sigma(\theta)$ and provide the specific loss function $L(\xi_\theta, \theta)$. Then, the formulation can be specialized to different learning modes, as discussed below.

IRL/IOC Mode. Suppose that we are given a demonstration $\xi^d = \{\mathbf{x}_{0:T}^d, \mathbf{u}_{0:T-1}^d\}$ of an unknown expert system, based on which we seek to learn the dynamics and control objective function of the expert. To this end, we use $\Sigma(\theta)$ (1) to represent the expert, and define the loss function (3) as

$$L(\xi_\theta, \theta) = \mathbb{E}_{\xi^d} [l(\xi_\theta, \xi^d)], \quad (4)$$

where l is a scalar function that penalizes the inconsistency of ξ_θ with ξ^d , e.g., $l(\xi_\theta, \xi^d) = \|\xi_\theta - \xi^d\|^2$. By solving (3), we can obtain a system $\Sigma(\theta)$ that is consistent with the observed demonstrations.

SysID Mode. Suppose that we are given input-output data $\xi^o = \{\mathbf{x}_{0:T}^o, \mathbf{u}_{0:T-1}^o\}$ recorded from, say, a physical system, and we wish to identify the system's dynamics equation. Here, inputs $\mathbf{u}_{0:T-1}$ are usually externally supplied to ensure the system is of persistent excitation [40]. In order for $\Sigma(\theta)$ in (1) to only represent a set of dynamics (since we do not care about its internal control law), we set $J(\theta) = 0$. Then its trajectory ξ_θ in (2) accepts any inputs $\mathbf{u}_{0:T-1}$ as it always optimizes $J(\theta) = 0$. In other words, by setting $J(\theta) = 0$, $\Sigma(\theta)$ in (1) now only represent a class of dynamics models:

$$\Sigma(\theta) : \quad \text{dynamics:} \quad \mathbf{x}_{t+1} = \mathbf{f}(\mathbf{x}_t, \mathbf{u}_t, \theta) \quad \text{with } \mathbf{x}_0 \text{ and external } \mathbf{u}_{0:T-1}. \quad (5)$$

Now, $\Sigma(\theta)$ in (5) will produce a trajectory $\xi_\theta = \{\mathbf{x}_{0:T}^\theta, \mathbf{u}_{0:T-1}^\theta\}$. To still use the problem formulation

in (3) for system identification, we define the loss function as

$$L(\xi_\theta, \theta) = \mathbb{E}_{\xi^o} [l(\xi_\theta, \xi^o)], \quad (6)$$

where l is a differentiable scalar-valued penalty function to quantify the reproduction error between the recorded data $\xi^o = \{x_{0:T}^o, u_{0:T-1}\}$ and simulated data $\xi_\theta = \{x_{0:T}^\theta, u_{0:T-1}\}$ under the same supplied inputs $u_{0:T-1}$.

Control/Planning Mode. For a system, given its dynamics learned via SysID Mode, we now want to design a control policy such that the system achieves a control performance of minimizing a cost function. In this case, we specialize the setting of $\Sigma(\theta)$ in (1) as follows: first, we set f as the learned dynamics and set $J(\theta) = 0$; and second, through a *feedback link*, we connect the control input u_t and state output x_t of $\Sigma(\theta)$ to an external block of a parameterized policy $u_t = u(t, x_t, \theta)$ (reminder: different from SysID Mode with control inputs supplied externally, the control inputs here are generated by a control policy via a feedback loop). The system $\Sigma(\theta)$ now becomes

$$\Sigma(\theta) : \begin{array}{l} \text{dynamics: } x_{t+1} = f(x_t, u_t) \text{ with } x_0, \\ \text{control policy: } u_t = u(t, x_t, \theta). \end{array} \quad (7)$$

Now, $\Sigma(\theta)$ in (7) will produce a trajectory $\xi_\theta = \{x_{0:T}^\theta, u_{0:T-1}^\theta\}$. We set the loss function in (3) as

$$L(\xi_\theta, \theta) = \sum_{t=0}^{T-1} l(x_t^\theta, u_t^\theta) + l_f(x_T^\theta), \quad (8)$$

where l and l_f are the stage and final cost functions, respectively. Then, (3) formulates an optimal control or planning problem, whose goal is to find an optimal policy. In fact, this learning mode can be used as a component to solve the optimal control system (1) in IRL/IOC Mode.

4 An End-to-End Learning Framework

To solve the general problem (3), the end-to-end learning optimizes the loss $L(\xi_\theta, \theta)$ directly with respect to the parameter of interest θ by applying the gradient descent,

$$\theta_{k+1} = \theta_k - \eta_k \frac{dL}{d\theta} \Big|_{\theta_k} \quad \text{with} \quad \frac{dL}{d\theta} \Big|_{\theta_k} = \frac{\partial L}{\partial \xi} \Big|_{\xi_{\theta_k}} \frac{\partial \xi_\theta}{\partial \theta} \Big|_{\theta_k} + \frac{\partial L}{\partial \theta} \Big|_{\theta_k}. \quad (9)$$

Here, $k = 0, 1, \dots$ is the iteration index; $\frac{dL}{d\theta} \Big|_{\theta_k}$ is the gradient of the loss with respect to θ evaluated at θ_k ; and η_k is the learning rate [41]. From (9), we can depict the overall learning pipeline in Fig. 2. Each update of θ consists of a *forward pass*, where at current θ_k , the trajectory ξ_{θ_k} is produced from $\Sigma(\theta_k)$ and the loss is solved, and a *backward pass*, where $\frac{\partial L}{\partial \xi} \Big|_{\xi_{\theta_k}}$, $\frac{\partial \xi_\theta}{\partial \theta} \Big|_{\theta_k}$, and $\frac{dL}{d\theta} \Big|_{\theta_k}$ are computed.

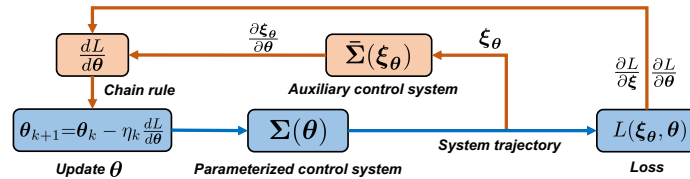


Figure 2: PDP end-to-end learning framework.

In the forward pass, ξ_θ is obtained by solving an optimal control system $\Sigma(\theta)$ using any available OC methods, such as iLQR or the Control/Planning Mode, (for SysID or Control modes, this is simply reduced to integration of difference equations (5) and (7)). In backward pass, $\frac{\partial L}{\partial \xi}$ and $\frac{\partial L}{\partial \theta}$ are obtained from the given loss function $L(\xi_\theta, \theta)$. The main challenge, however, is to solve $\frac{\partial \xi_\theta}{\partial \theta}$, i.e., the *gradient/variation of trajectory with respect to the parameter of the system*. Next, we will analytically solve $\frac{\partial \xi_\theta}{\partial \theta}$ by proposing two techniques: the *differential PMP* and *auxiliary control system*.

5 Key Contributions: Differential PMP & Auxiliary Control System

We first recall the discrete-time Pontryagin's Maximum Principle (PMP) [29] (a derivation of the discrete-time PMP is given in Appendix C). For the optimal control system $\Sigma(\theta)$ in (1) with a fixed θ ,

the PMP describes a set of optimality conditions which the system trajectory $\xi_\theta = \{x_{0:T}^\theta, u_{0:T-1}^\theta\}$ (2) must satisfy. To introduce these conditions, we first defining the following *Hamiltonian*,

$$H_t = c_t(x_t, u_t; \theta) + f(x_t, u_t; \theta)' \lambda_{t+1}, \quad (10)$$

where $\lambda_t \in \mathbb{R}^n$ ($t = 1, 2, \dots, T$) is called the *costate variable*, which can be also thought of as the Lagrange multipliers for the dynamics constraints. According to the PMP, there exist a sequence of costates $\lambda_{1:T}^\theta$, which together with the system optimal trajectory $\xi_\theta = \{x_{0:T}^\theta, u_{0:T-1}^\theta\}$ satisfy

$$\text{dynamics equation: } x_{t+1}^\theta = \frac{\partial H_t}{\partial \lambda_{t+1}^\theta} = f(x_t^\theta, u_t^\theta; \theta), \quad (11a)$$

$$\text{costate equation: } \lambda_t^\theta = \frac{\partial H_t}{\partial x_t^\theta} = \frac{\partial c_t}{\partial x_t^\theta} + \frac{\partial f'}{\partial x_t^\theta} \lambda_{t+1}^\theta, \quad (11b)$$

$$\text{input equation: } 0 = \frac{\partial H_t}{\partial u_t^\theta} = \frac{\partial c_t}{\partial u_t^\theta} + \frac{\partial f'}{\partial u_t^\theta} \lambda_{t+1}^\theta, \quad (11c)$$

$$\text{boundary condition: } \lambda_T^\theta = \frac{\partial h}{\partial x_T^\theta}. \quad (11d)$$

For notation simplicity, $\frac{\partial g}{\partial x_t}$ means derivative of a function $g(x)$ with respect to x evaluated at x_t .

5.1 Differential PMP

To begin, recall that our goal (in Section 4) is to obtain $\frac{\partial \xi_\theta}{\partial \theta}$, that is,

$$\frac{\partial \xi_\theta}{\partial \theta} = \left\{ \frac{\partial x_{0:T}^\theta}{\partial \theta}, \frac{\partial u_{0:T-1}^\theta}{\partial \theta} \right\}. \quad (12)$$

To this end, we are motivated to differentiate the PMP conditions in (11) on both sides with respect to θ , respectively. This leads to the following *differential PMP*:

$$\text{differential dynamics equation: } \frac{\partial x_{t+1}^\theta}{\partial \theta} = F_t \frac{\partial x_t^\theta}{\partial \theta} + G_t \frac{\partial u_t^\theta}{\partial \theta} + E_t, \quad (13a)$$

$$\text{differential costate equation: } \frac{\partial \lambda_t^\theta}{\partial \theta} = H_t^{xx} \frac{\partial x_t^\theta}{\partial \theta} + H_t^{xu} \frac{\partial u_t^\theta}{\partial \theta} + F_t' \frac{\partial \lambda_{t+1}^\theta}{\partial \theta} + H_t^{xe}, \quad (13b)$$

$$\text{differential input equation: } 0 = H_t^{ux} \frac{\partial x_t^\theta}{\partial \theta} + H_t^{uu} \frac{\partial u_t^\theta}{\partial \theta} + G_t' \frac{\partial \lambda_{t+1}^\theta}{\partial \theta} + H_t^{ue}, \quad (13c)$$

$$\text{differential boundary condition: } \frac{\partial \lambda_T^\theta}{\partial \theta} = H_T^{xx} \frac{\partial x_T^\theta}{\partial \theta} + H_T^{xe}, \quad (13d)$$

Here, to simplify notations and distinguish knowns and unknowns, the coefficient matrices in the above differential PMP (13) are defined as follows:

$$F_t = \frac{\partial f}{\partial x_t^\theta}, \quad G_t = \frac{\partial f}{\partial u_t^\theta}, \quad H_t^{xx} = \frac{\partial^2 H_t}{\partial x_t^\theta \partial x_t^\theta}, \quad H_t^{xe} = \frac{\partial^2 H_t}{\partial x_t^\theta \partial \theta}, \quad H_t^{xu} = \frac{\partial^2 H_t}{\partial x_t^\theta \partial u_t^\theta} = (H_t^{ux})', \quad (14a)$$

$$E_t = \frac{\partial f}{\partial \theta}, \quad H_t^{uu} = \frac{\partial^2 H_t}{\partial u_t^\theta \partial u_t^\theta}, \quad H_t^{ue} = \frac{\partial^2 H_t}{\partial u_t^\theta \partial \theta}, \quad H_T^{xx} = \frac{\partial^2 h}{\partial x_T^\theta \partial x_T^\theta}, \quad H_T^{xe} = \frac{\partial^2 h}{\partial x_T^\theta \partial \theta}, \quad (14b)$$

where we use $\frac{\partial^2 g}{\partial x_t \partial u_t}$ to denote the second-order derivative of a function $g(x, u)$ evaluated at (x_t, u_t) .

Since the system trajectory $\xi_\theta = \{x_{0:T}^\theta, u_{0:T-1}^\theta\}$ is obtained in the forward pass (recall Fig. 2), all matrices in (14) are thus known (note that the computation of these matrices also requires $\lambda_{1:T}^\theta$, which can be obtained by iteratively solving (11b) and (11d) given ξ_θ). From the differential PMP (13), we note that to obtain $\frac{\partial \xi_\theta}{\partial \theta}$ in (12), it is sufficient to compute the unknowns $\left\{ \frac{\partial x_{0:T}^\theta}{\partial \theta}, \frac{\partial u_{0:T-1}^\theta}{\partial \theta}, \frac{\partial \lambda_{1:T}^\theta}{\partial \theta} \right\}$ in (13). Next we will show that how these unknowns are elegantly solved by proposing another system.

5.2 Auxiliary Control System

One important observation to the differential PMP (13) is that it shares a similar structure to the original PMP (11), so it can be viewed as a new set of PMP equations corresponding to an ‘oracle control optimal system’ whose the ‘optimal trajectory’ is exactly (12). This motivate us to ‘unearth’ this oracle optimal control system, because by doing so, (12) can be obtained from this oracle system using any OC solver. To this end, we first define the new ‘state’ and ‘control’ (matrix) variables:

$$X_t = \frac{\partial x_t}{\partial \theta} \in \mathbb{R}^{n \times r}, \quad U_t = \frac{\partial u_t}{\partial \theta} \in \mathbb{R}^{m \times r}, \quad (15)$$

respectively. Then we ‘artificially’ define the following *auxiliary control system* $\bar{\Sigma}(\xi_\theta)$:

$$\bar{\Sigma}(\xi_\theta) : \begin{array}{l} \text{dynamics: } X_{t+1} = F_t X_t + G_t U_t + E_t \quad \text{with } X_0 = \mathbf{0}, \\ \text{control objective: } \bar{J} = \text{Tr} \sum_{t=0}^{T-1} \left(\frac{1}{2} \begin{bmatrix} X_t \\ U_t \end{bmatrix}' \begin{bmatrix} H_t^{xx} & H_t^{xu} \\ H_t^{ux} & H_t^{uu} \end{bmatrix} \begin{bmatrix} X_t \\ U_t \end{bmatrix} + \begin{bmatrix} H_t^{xe} \\ H_t^{ue} \end{bmatrix}' \begin{bmatrix} X_t \\ U_t \end{bmatrix} \right) \\ \quad + \text{Tr} \left(\frac{1}{2} X_T' H_T^{xx} U_T + (H_T^{xe})' X_T \right). \end{array} \quad (16)$$

Here, $X_0 = \frac{\partial \mathbf{x}_0}{\partial \theta} = \mathbf{0}$ because \mathbf{x}_0 in (1) is given; \bar{J} is the defined control objective function which needs to be optimized in the auxiliary control system; and Tr denotes matrix trace. Before presenting the key result, we make some comments on the above proposed auxiliary control system $\bar{\Sigma}(\xi_\theta)$. First, its state and control variables are both matrix variables defined in (15). Second, its dynamics is linear and control objective function \bar{J} is quadratic, for which the coefficient matrices are given in (14). Third, its dynamics and objective function are determined by the trajectory ξ_θ of the system $\Sigma(\theta)$ in forward pass, and this is why we denote it as $\bar{\Sigma}(\xi_\theta)$. Finally, we have the following important result.

Lemma 5.1. *Let $\{X_{0:T}^\theta, U_{0:T-1}^\theta\}$ be a stationary solution to the auxiliary control system $\bar{\Sigma}(\xi_\theta)$ (16). Then, $\{X_{0:T}^\theta, U_{0:T-1}^\theta\}$ satisfies the Pontryagin’s Maximum Principle of $\Sigma(\xi_\theta)$, which is (13), and*

$$\{X_{0:T}^\theta, U_{0:T-1}^\theta\} = \left\{ \frac{\partial \mathbf{x}_{0:T}}{\partial \theta}, \frac{\partial \mathbf{u}_{0:T-1}}{\partial \theta} \right\} = \frac{\partial \xi_\theta}{\partial \theta}. \quad (17)$$

A proof of Lemma 5.1 is in Appendix A. Lemma 5.1 states two assertions. First, the PMP condition for the auxiliary control system $\bar{\Sigma}(\xi_\theta)$ is exactly the differential PMP (13) for the original system $\Sigma(\theta)$; and second, importantly, the trajectory $\{X_{0:T}^\theta, U_{0:T-1}^\theta\}$ produced by the auxiliary control system $\bar{\Sigma}(\xi_\theta)$ is exactly the gradient of trajectory of the original system $\Sigma(\theta)$ with respect to the parameter θ . Due to Lemma 5.1, we can obtain $\frac{\partial \xi_\theta}{\partial \theta}$ from $\bar{\Sigma}(\xi_\theta)$ efficiently using the lemma below.

Lemma 5.2. *If H_t^{uu} in (16) is invertible for all $t = 0, 1, \dots, T-1$, define the following recursions*

$$P_t = Q_t + A_t'(I + P_{t+1}R_t)^{-1}P_{t+1}A_t, \quad (18a)$$

$$W_t = A_t'(I + P_{t+1}R_t)^{-1}(W_{t+1} + P_{t+1}M_t) + N_t, \quad (18b)$$

with $P_T = H_T^{xx}$ and $W_T = H_T^{xe}$. Here, I is identity matrix, $A_t = F_t - G_t(H_t^{uu})^{-1}H_t^{ux}$, $R_t = G_t(H_t^{uu})^{-1}G_t'$, $M_t = E_t - G_t(H_t^{uu})^{-1}H_t^{ue}$, $Q_t = H_t^{xx} - H_t^{xu}(H_t^{uu})^{-1}H_t^{ux}$, $N_t = H_t^{xe} - H_t^{xu}(H_t^{uu})^{-1}H_t^{ue}$ are all known given (14). Then, the stationary solution $\{X_{0:T}^\theta, U_{0:T-1}^\theta\}$ in (17) can be obtained by iteratively solving the following equations from $t = 0$ to $T-1$ with $X_0^\theta = X_0 = \mathbf{0}$:

$$U_t^\theta = -(H_t^{uu})^{-1} \left(H_t^{ux} X_t^\theta + H_t^{ue} + G_t'(I + P_{t+1}R_t)^{-1} (P_{t+1}A_t X_t^\theta + P_{t+1}M_t + W_{t+1}) \right), \quad (19a)$$

$$X_{t+1}^\theta = F_t X_t^\theta + G_t U_t^\theta + E_t. \quad (19b)$$

A proof of Lemma 5.2 is in Appendix B. Lemma 5.2 states that the trajectory of the auxiliary control system $\bar{\Sigma}(\xi_\theta)$ can be obtained by two steps: first, iteratively solve the equations (18) backward in time to obtain the matrices P_t and W_t (all other coefficient matrices are known given $\bar{\Sigma}(\xi_\theta)$); second, calculate $\{X_{0:T}^\theta, U_{0:T-1}^\theta\}$ by iteratively integrating a feedback-control system (19) forward in time. In fact, these two steps are standard procedures to solve general finite-time LQR problems [42].

As a conclusion to the techniques developed in Section 5, we summarize the procedure of computing $\frac{\partial \xi_\theta}{\partial \theta}$ using the proposed auxiliary control system in Algorithm 1. This algorithm serves as a key component in the backward pass of the PDP learning framework, as shown in Fig. 2.

Algorithm 1: Solving $\frac{\partial \xi_\theta}{\partial \theta}$ using Auxiliary Control System (See detailed version in Appendix D)

Input: The trajectory ξ_θ (2) produced by the system $\Sigma(\theta)$ in (1) in forward pass.

 Compute the coefficient matrices (14) to obtain the auxiliary control system $\bar{\Sigma}(\xi_\theta)$ in (16);

 Solve the auxiliary control system $\bar{\Sigma}(\xi_\theta)$ to obtain $\{X_{0:T}^\theta, U_{0:T-1}^\theta\}$ using Lemma 5.2;

Return: $\frac{\partial \xi_\theta}{\partial \theta} = \{X_{0:T}^\theta, U_{0:T-1}^\theta\}$

6 Applications to Different Learning Modes and Experiments

We investigate three learning modes of the PDP, as described in Section 3. For each mode, we demonstrate its capability on four systems (Table 2): cartpole, multilink robot arm, a 6 DoF maneuvering UAV, and the more challenging 6 DoF rocket powered landing. In each task, a learning baseline and a state-of-the-art method are compared. Please see algorithm and experiment details in Appendix D and E, respectively. Complexity and limitation are analyzed in Appendix G/F and H, respectively.

Table 2: Experimental systems (results for 6-DoF rocket powered landing is in Appendix I)

Systems	Dynamics parameter θ_{dyn}	Control objective parameter θ_{obj}
Cartpole	cart mass, pole mass and length	
Multi-link robot arm	length and mass for each link	$c(\mathbf{x}, \mathbf{u}) = \ \theta'_{\text{obj}}(\mathbf{x} - \mathbf{x}_g)\ ^2 + \ \mathbf{u}\ ^2$
6-DoF UAV maneuvering	mass, wing length, inertia matrix	$h(\mathbf{x}, \mathbf{u}) = \ \theta'_{\text{obj}}(\mathbf{x} - \mathbf{x}_g)\ ^2$
6-DoF rocket powered landing	mass, rocket length, inertia matrix	

We fix the weight to $\|\mathbf{u}\|^2$, because estimating all weights will incur ambiguity [35]; \mathbf{x}_g is the goal state.

IRL/IOC Mode. The parameterized system $\Sigma(\theta)$ is (1) and loss is (4). In forward pass of the PDP framework, ξ_θ is solved from $\Sigma(\theta)$ by any (external) OC solver. In backward pass, $\frac{\partial \xi_\theta}{\partial \theta}$ is computed from the auxiliary control system $\bar{\Sigma}(\xi_\theta)$ (16) by Algorithm 1. The entire algorithm is in Appendix D.

Experiments: imitation learning. We use IRL/IOC Mode to solve imitation learning for the systems in Table 2. The true dynamics is parameterized, and the control objective is parameterized as a weighted distance to the goal, $\theta = \{\theta_{\text{dyn}}, \theta_{\text{obj}}\}$. Set imitation loss $L(\xi_\theta, \theta) = \mathbb{E}_{\xi^d} \|\xi^d - \xi_\theta\|^2$. Two other methods are compared: (i) neural policy imitation/cloning, and (ii) inverse KKT [39] (see Appendix E). We set learning rate $\eta = 10^{-4}$ for all methods and run five trials with random initial guess θ_0 . The results are in Fig. 3.

Fig. 3a-3c shows that the PDP significantly outperforms the neural policy imitation and inverse-KKT method, and shows a much lower training loss and much faster convergence. To validate the learned model, we use it to perform motion planning for the UAV in unseen settings, and the resulting control trajectory is plotted in Fig. 3d. The result shows that compared to other two methods, the PDP accurately predicts the expert’s trajectory in new settings, which shows its better generality than the other two. Please refer to Appendix E for more details (see video demos at [link](#)).

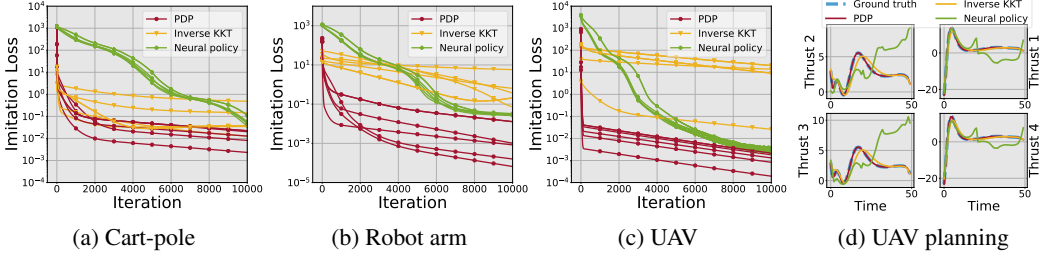


Figure 3: (a-c) imitation loss versus iteration, (d) planning in unseen settings using learned models.

SysID Mode: The parameterized system $\Sigma(\theta)$ is (5) and loss is (6). The PDP in this mode is greatly simplified. In forward pass, ξ_θ is solved by integrating the difference equation (5). In backward pass, the auxiliary control system (16) is reduced to

$$\bar{\Sigma}(\xi_\theta) : \quad \text{dynamics: } X_{t+1}^\theta = F_t X_t^\theta + E_t \quad \text{with } X_0 = \mathbf{0}. \quad (20)$$

This is because $\Sigma(\theta)$ in (5) results from letting $J(\theta) = 0$, (13b-13d) and \bar{J} in (16) are then trivialized, and also because $\mathbf{u}_{0:T-1}$ is given in (5), thus $U_t^\theta = \mathbf{0}$ in (13a). By integrating (20) from $t = 0$ to T , one obtains $X_{0:T}^\theta = \frac{\partial \xi_\theta}{\partial \theta}$. The entire algorithm is in Appendix D.

Experiment: system identification. We use the SysID Mode to identify the dynamics parameter θ_{dyn} of the systems in Table 2. Set the SysID loss $L(\xi_\theta, \theta) = \mathbb{E}_{\xi^o} \|\xi^o - \xi_\theta\|^2$. Two other methods are compared: (i) training a neural dynamics model, and (ii) DMDc [43] (see Appendix E). For all methods, we set learning rate $\eta = 10^{-4}$, and run five trials with random θ_0 . The results are in Fig. 4.

Fig. 4a-4c shows an obvious advantage of the PDP over the neural-network baseline and DMDc in terms of lower training loss and faster convergence speed. To validate the learned dynamics, we use

it to predict the motion of the unactuated cartpole, and the results are in Fig. 4d. The results show the model learned by the PDP can accurately predict the free motion, while neural models and DMDC shows a low accuracy. More information is in Appendix E (see video demos at [link](#)).

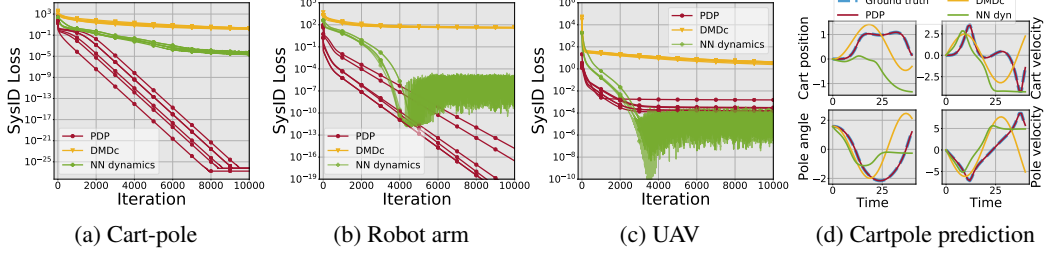


Figure 4: (a-c) SysID loss versus iteration, (d) motion prediction using the learned dynamics.

Control/Planning Mode: The parameterized system $\Sigma(\theta)$ is (7) and loss is (8). The PDP for this mode is also simplified. In forward pass, ξ_θ is solved by integrating a (controlled) difference equation (7). In backward pass, \bar{J} in the auxiliary control system (16) is trivialized because we have considered $J(\theta) = 0$ in (7). Since the control is now given by $u_t = u(t, x_t, \theta)$, U_t^θ is obtained by differentiating the policy on both side with respect to θ , that is, $U_t^\theta = U_x X_t^\theta + U_e$ with $U_x = \frac{\partial u}{\partial x}$ and $U_e = \frac{\partial u}{\partial \theta}$. Thus,

$$\bar{\Sigma}(\xi_\theta) : \begin{array}{l} \text{dynamics: } X_{t+1}^\theta = F_t X_t^\theta + G_t U_t^\theta \text{ with } X_0 = \mathbf{0}, \\ \text{control policy: } U_t^\theta = U_x X_t^\theta + U_e. \end{array} \quad (21)$$

Integrating (21) from $t = 0$ to T leads to $\{X_{0:T}^\theta, U_{0:T-1}^\theta\} = \frac{\partial \xi_\theta}{\partial \theta}$. The algorithm is in Appendix D.

Experiments: optimal control. Based on the dynamics identified in SysID Mode, we learn a policy for the systems in Table 2 to optimize a control objective of a given θ_{obj} . Set the loss (8) exactly as the control objective (below referred to as control loss). We use the Lagrange polynomial of degree N (see Appendix E) to parameterize the policy. iLQR [28] and an OC solver [44] are compared. We use the learning rate $\eta = 10^{-4}$ for both PDP and iLQR, and run five trials. The results are in Fig. 5.

Fig. 5a-5b show that the PDP has a much faster convergence than iLQR, and successfully converges to minimal control loss. Since the PDP minimizes the control loss over a parameterized policy, the accuracy of solution depends on specific parameterization (expressive power). As in Fig. 5d, the use of polynomial policy of degree $N = 35$ obtains a trajectory much closer to the ground truth than the use of $N = 5$. iLQR directly optimizes over control trajectory and generally has high accuracy (see Fig. 5d), but with high computational cost. More details are in Appendix E (see video demos at [link](#)).

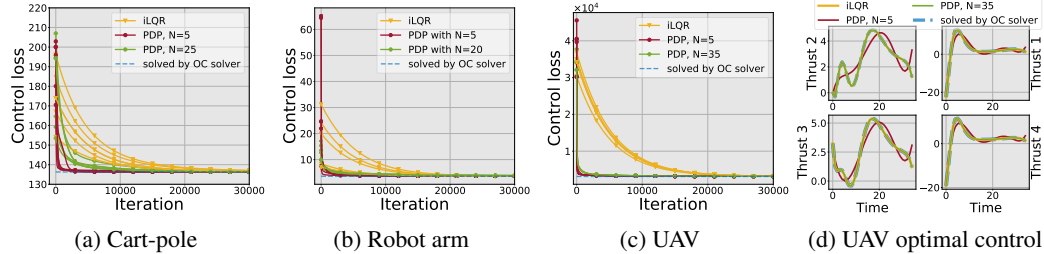


Figure 5: (a-c) control loss versus iteration, (d) the obtained control trajectories.

7 Conclusions

This paper proposes a Pontryagin differentiable programming (PDP) methodology to establish an end-to-end framework for solving a range of learning and control tasks. The PDP features two techniques: one is differentiation of the Pontryagin’s Maximum Principle, and the other is the auxiliary control system in backward pass of learning, and those two techniques are our contributions to both learning and control fields. We investigate three learning modes of the PDP: inverse reinforcement learning, system identification, and control/planning, respectively. For each learning mode of the PDP, we demonstrate its capability using several challenging high-dimensional systems such as UAV 6-DoF maneuvering and 6-DoF rocket powered landing. We envision the proposed PDP could benefit to both the learning and control communities for solving high-dimensional continuous-space problems.

Broader Impact

This work is expected to have the impacts on both the learning and control research.

- To the learning area, this work develops a principled framework that is flexible to solve a broad range of learning and control tasks, including system identification, control/planning, inverse reinforcement learning. A key contribution is that we propose a trajectory perspective for learning, and show how to integrate control theory into the learning framework. Because of this, the PDP shows advantage of sample, computation- and memory-cost efficiency over other learning methods (see comparison and analysis with other frameworks in Appendix F). More importantly, PDP has demonstrated capability to solve challenging high-dimensional and continuous-space tasks, such as 6-DoF UAV maneuvering and 6-DoF rocket powered landing.
- To the control area, this work proposes a general paradigm, which shows how complex control tasks can be transformed into learning problems and then solved by learning techniques. For example, we use the proposed PDP learning framework to solve system identification and optimal control problems, for both of which, the PDP shows advantage of efficiently handling non-linear systems over the state-of-the-art control methods. Since control theory typically requires knowledge of systems models, we expect that this work could extend the classic control theory by combining it with data-driven techniques.
- This paper has the theoretical contributions both to learning and control areas. As discussed in Section 2, to authors' best knowledge in learning and control, this work first proposes the techniques of differentiation/variation of the Pontryagin's Maximum Principle, which leads to the analytical gradient of (optimal) trajectory with respect to the tunable parameter of an (optimal) control system. Second, to our best knowledge, this is the first paper to introduce the auxiliary control system in backward pass of learning, and we theoretically prove that the differentiation of PMP is equivalent to the solution to the auxiliary control system.

Since we have not considered boundness constraints of a system in our formulation, the real-world use of this work on physical systems might possibly raise safety issues during the training process; e.g., the state or input of the physical system at some time instance might exceed the safety bounds that is physically required. One option to address this is to include these safety constraints as soft constraints added to the control objective or loss that is optimized. In future work, we will formally discuss the PDP framework within a safety framework. The proposed methods in this work, including the numerical experiments, do not leverage any bias in data.

References

- [1] Marc Deisenroth and Carl E Rasmussen. Pilco: A model-based and data-efficient approach to policy search. In *International Conference on Machine Learning*, pages 465–472, 2011.
- [2] Nicolas Heess, Gregory Wayne, David Silver, Timothy Lillicrap, Tom Erez, and Yuval Tassa. Learning continuous control policies by stochastic value gradients. In *Advances in Neural Information Processing Systems*, pages 2944–2952, 2015.
- [3] Joshua L Proctor, Steven L Brunton, and J Nathan Kutz. Generalizing koopman theory to allow for inputs and control. *SIAM Journal on Applied Dynamical Systems*, 17(1):909–930, 2018.
- [4] Ian Abraham and Todd D Murphey. Active learning of dynamics for data-driven control using koopman operators. *IEEE Transactions on Robotics*, 35(5):1071–1083, 2019.
- [5] Rolf Johansson. *System modeling and identification*. Prentice Hall, 1993.
- [6] Bernard O Koopman. Hamiltonian systems and transformation in hilbert space. *Proceedings of the National Academy of Sciences of the United States of America*, 17(5):315, 1931.
- [7] Matthew O Williams, Ioannis G Kevrekidis, and Clarence W Rowley. A data-driven approximation of the koopman operator: Extending dynamic mode decomposition. *Journal of Nonlinear Science*, 25(6):1307–1346, 2015.

- [8] Bethany Lusch, J Nathan Kutz, and Steven L Brunton. Deep learning for universal linear embeddings of nonlinear dynamics. *Nature communications*, 9(1):1–10, 2018.
- [9] Steven L Brunton, Joshua L Proctor, and J Nathan Kutz. Discovering governing equations from data by sparse identification of nonlinear dynamical systems. *Proceedings of the national academy of sciences*, 113(15):3932–3937, 2016.
- [10] Lennart Ljung and Torkel Glad. *Modeling of dynamic systems*. 1994.
- [11] Tian Qi Chen, Yulia Rubanova, Jesse Bettencourt, and David K Duvenaud. Neural ordinary differential equations. In *Advances in Neural Information Processing Systems*, pages 6571–6583, 2018.
- [12] Jiequn Han and Weinan E. Deep learning approximation for stochastic control problems. *Deep Reinforcement Learning Workshop, Advances in Neural Information Processing Systems*, 2016.
- [13] Qianxiao Li, Long Chen, Cheng Tai, and E Weinan. Maximum principle based algorithms for deep learning. *Journal of Machine Learning Research*, 18(1):5998–6026, 2017.
- [14] Qianxiao Li and Shuji Hao. An optimal control approach to deep learning and applications to discrete-weight neural networks. *arXiv preprint arXiv:1803.01299*, 2018.
- [15] Weinan E, Jiequn Han, and Qianxiao Li. A mean-field optimal control formulation of deep learning. *Research in the Mathematical Sciences*, 6(1), 2019.
- [16] Dinghuai Zhang, Tianyuan Zhang, Yiping Lu, Zhanxing Zhu, and Bin Dong. You only propagate once: Painless adversarial training using maximal principle. *arXiv preprint arXiv:1905.00877*, 2019.
- [17] Martin Benning, Elena Celledoni, Matthias J Ehrhardt, Brynjulf Owren, and Carola-Bibiane Schönlieb. Deep learning as optimal control problems: models and numerical methods. *arXiv preprint arXiv:1904.05657*, 2019.
- [18] Hailiang Liu and Peter Markowich. Selection dynamics for deep neural networks. *arXiv preprint arXiv:1905.09076*, 2019.
- [19] Guan-Horng Liu and Evangelos A Theodorou. Deep learning theory review: An optimal control and dynamical systems perspective. *arXiv preprint arXiv:1908.10920*, 2019.
- [20] Junhyuk Oh, Valliappa Chockalingam, Satinder Singh, and Honglak Lee. Control of memory, active perception, and action in minecraft. *arXiv preprint arXiv:1605.09128*, 2016.
- [21] Volodymyr Mnih, Koray Kavukcuoglu, David Silver, Alex Graves, Ioannis Antonoglou, Daan Wierstra, and Martin Riedmiller. Playing atari with deep reinforcement learning. *arXiv preprint arXiv:1312.5602*, 2013.
- [22] Volodymyr Mnih, Koray Kavukcuoglu, David Silver, Andrei A Rusu, Joel Veness, Marc G Bellemare, Alex Graves, Martin Riedmiller, Andreas K Fidjeland, Georg Ostrovski, et al. Human-level control through deep reinforcement learning. *Nature*, 518(7540):529, 2015.
- [23] Jeff G Schneider. Exploiting model uncertainty estimates for safe dynamic control learning. In *Advances in Neural Information Processing Systems*, pages 1047–1053, 1997.
- [24] Pieter Abbeel, Morgan Quigley, and Andrew Y Ng. Using inaccurate models in reinforcement learning. In *International Conference on Machine Learning*, pages 1–8, 2006.
- [25] Kendall Lowrey, Aravind Rajeswaran, Sham Kakade, Emanuel Todorov, and Igor Mordatch. Plan online, learn offline: Efficient learning and exploration via model-based control. *arXiv preprint arXiv:1811.01848*, 2018.
- [26] Jiongmin Yong and Xun Yu Zhou. *Stochastic controls: Hamiltonian systems and HJB equations*, volume 43. Springer Science & Business Media, 1999.
- [27] David H Jacobson and David Q Mayne. *Differential dynamic programming*. 1970.

- [28] Weiwei Li and Emanuel Todorov. Iterative linear quadratic regulator design for nonlinear biological movement systems. In *International Conference on Informatics in Control, Automation and Robotics*, pages 222–229, 2004.
- [29] Lev Semenovich Pontryagin, V. G. Boltyanskiy, R. V. Gamkrelidze, and E. F. Mishchenko. *The Mathematical Theory of Optimal Processes*. John Wiley & Sons, Inc., 1962.
- [30] Hans Georg Bock and Karl-Josef Plitt. A multiple shooting algorithm for direct solution of optimal control problems. In *IFAC World Congress: A Bridge Between Control Science and Technology*, pages 1603–1608, 1984.
- [31] Michael A Patterson and Anil V Rao. Gpops-ii: A matlab software for solving multiple-phase optimal control problems using hp-adaptive gaussian quadrature collocation methods and sparse nonlinear programming. *ACM Transactions on Mathematical Software*, 41(1):1, 2014.
- [32] Pieter Abbeel and Andrew Y Ng. Apprenticeship learning via inverse reinforcement learning. In *International Conference on Machine Learning*, pages 1–8, 2004.
- [33] Brian D Ziebart, Andrew Maas, J Andrew Bagnell, and Anind K Dey. Maximum entropy inverse reinforcement learning. In *AAAI Conference on Artificial Intelligence*, pages 1433–1438, 2008.
- [34] Nathan D Ratliff, J Andrew Bagnell, and Martin A Zinkevich. Maximum margin planning. In *International Conference on Machine Learning*, pages 729–736, 2006.
- [35] Arezou Keshavarz, Yang Wang, and Stephen Boyd. Imputing a convex objective function. In *IEEE International Symposium on Intelligent Control*, pages 613–619, 2011.
- [36] Katja Mombaur, Anh Truong, and Jean-Paul Laumond. From human to humanoid locomotion—an inverse optimal control approach. *Autonomous Robots*, 28(3):369–383, 2010.
- [37] Wanxin Jin, Dana Kulić, Shaoshuai Mou, and Sandra Hirche. Inverse optimal control with incomplete observations. *arXiv preprint arXiv:1803.07696*, 2018.
- [38] Wanxin Jin, Dana Kulić, Jonathan Feng-Shun Lin, Shaoshuai Mou, and Sandra Hirche. Inverse optimal control for multiphase cost functions. *IEEE Transactions on Robotics*, 35(6):1387–1398, 2019.
- [39] Peter Englert, Ngo Anh Vien, and Marc Toussaint. Inverse kkt: Learning cost functions of manipulation tasks from demonstrations. *The International Journal of Robotics Research*, 36(13-14):1474–1488, 2017.
- [40] Michael Green and John B Moore. Persistence of excitation in linear systems. *Systems & control letters*, 7(5):351–360, 1986.
- [41] Matthew D Zeiler. Adadelta: an adaptive learning rate method. *arXiv preprint arXiv:1212.5701*, 2012.
- [42] Huibert Kwakernaak and Raphael Sivan. *Linear optimal control systems*, volume 1. New York: Wiley-Interscience, 1972.
- [43] Joshua L Proctor, Steven L Brunton, and J Nathan Kutz. Dynamic mode decomposition with control. *SIAM Journal on Applied Dynamical Systems*, 15(1):142–161, 2016.
- [44] Joel A E Andersson, Joris Gillis, Greg Horn, James B Rawlings, and Moritz Diehl. CasADi – A software framework for nonlinear optimization and optimal control. *Mathematical Programming Computation*, 11(1):1–36, 2019.
- [45] Michael Athans. The matrix minimum principle. *Information and Control*, 11(5-6):592–606, 1967.
- [46] Mordecai Avriel. *Nonlinear programming: analysis and methods*. Courier Corporation, 2003.
- [47] Daniel Liberzon. *Calculus of variations and optimal control theory: a concise introduction*. Princeton University Press, 2011.

- [48] Brandon Amos, Ivan Jimenez, Jacob Sacks, Byron Boots, and J Zico Kolter. Differentiable mpc for end-to-end planning and control. In *Advances in Neural Information Processing Systems*, pages 8289–8300, 2018.
- [49] Jack B Kuipers. *Quaternions and rotation sequences*, volume 66. Princeton University Press, 1999.
- [50] Taeyoung Lee, Melvin Leok, and N Harris McClamroch. Geometric tracking control of a quadrotor uav on $se(3)$. In *IEEE Conference on Decision and Control*, pages 5420–5425, 2010.
- [51] Mark W Spong and Mathukumalli Vidyasagar. *Robot dynamics and control*. John Wiley & Sons, 2008.
- [52] Mariusz Bojarski, Davide Del Testa, Daniel Dworakowski, Bernhard Firner, Beat Flepp, Praseon Goyal, Lawrence D Jackel, Mathew Monfort, Urs Muller, Jiakai Zhang, et al. End to end learning for self-driving cars. *arXiv preprint arXiv:1604.07316*, 2016.
- [53] Milton Abramowitz and Irene A Stegun. *Handbook of mathematical functions with formulas, graphs, and mathematical tables*, volume 55. U.S. Government Printing Office, 1948.
- [54] Gamal Elnagar, Mohammad A Kazemi, and Mohsen Razzaghi. The pseudospectral legendre method for discretizing optimal control problems. *IEEE Transactions on Automatic Control*, 40(10):1793–1796, 1995.
- [55] Masashi Okada, Luca Rigazio, and Takenobu Aoshima. Path integral networks: End-to-end differentiable optimal control. *arXiv preprint arXiv:1706.09597*, 2017.
- [56] Marcus Pereira, David D Fan, Gabriel Nakajima An, and Evangelos Theodorou. Mpc-inspired neural network policies for sequential decision making. *arXiv preprint arXiv:1802.05803*, 2018.
- [57] Hilbert J Kappen. Path integrals and symmetry breaking for optimal control theory. *Journal of Statistical Mechanics: Theory and Experiment*, 2005.
- [58] Martín Abadi, Ashish Agarwal, Paul Barham, Eugene Brevdo, Zhifeng Chen, Craig Citro, Greg S Corrado, Andy Davis, Jeffrey Dean, Matthieu Devin, et al. Tensorflow: Large-scale machine learning on heterogeneous distributed systems. *arXiv preprint arXiv:1603.04467*, 2016.
- [59] Aravind Srinivas, Allan Jabri, Pieter Abbeel, Sergey Levine, and Chelsea Finn. Universal planning networks. *arXiv preprint arXiv:1804.00645*, 2018.
- [60] Aviv Tamar, Garrett Thomas, Tianhao Zhang, Sergey Levine, and Pieter Abbeel. Learning from the hindsight plan—episodic mpc improvement. In *IEEE International Conference on Robotics and Automation*, pages 336–343, 2017.
- [61] Peng Xu, Fred Roosta, and Michael W Mahoney. Second-order optimization for non-convex machine learning: An empirical study. In *SIAM International Conference on Data Mining*, pages 199–207, 2020.
- [62] Michael Szmuk and Behcet Acikmese. Successive convexification for 6-dof mars rocket powered landing with free-final-time. In *AIAA Guidance, Navigation, and Control Conference*, page 0617, 2018.

A Proof of Lemma 5.1

To prove Lemma 5.1, we just needs to show that the Pontryagin's Maximum Principle for the auxiliary control system $\bar{\Sigma}(\xi_\theta)$ in (16) is exactly the differential PMP equations in (13). To this end, we define the following Hamiltonian for the auxiliary control system:

$$\bar{H}_t = \text{Tr} \left(\frac{1}{2} \begin{bmatrix} X_t \\ U_t \end{bmatrix}' \begin{bmatrix} H_t^{xx} & H_t^{xu} \\ H_t^{ux} & H_t^{uu} \end{bmatrix} \begin{bmatrix} X_t \\ U_t \end{bmatrix} + \begin{bmatrix} H_t^{xe} \\ H_t^{ue} \end{bmatrix}' \begin{bmatrix} X_t \\ U_t \end{bmatrix} \right) + \text{Tr} (\Lambda'_{t+1} (F_t X_t + G_t U_t + E_t)), \quad (\text{A.1})$$

with $t = 0, 1, \dots, T-1$. Here $\Lambda_{t+1} \in \mathbb{R}^{n \times r}$ denotes the costate (matrix) variables for the auxiliary control system. Based on Section 3 in [45], there exists a sequence of costates $\Lambda_{1:T}^\theta$, which together the stationary solution $\{X_{0:T}^\theta, U_{0:T-1}^\theta\}$ of the auxiliary control system must satisfy the following the matrix version of PMP (we here use the notation style similar to (11)).

The dynamics equation:

$$\begin{aligned} \frac{\partial \bar{H}_t}{\partial \Lambda_{t+1}^\theta} &= \frac{\partial \text{Tr} (\Lambda'_{t+1} (F_t X_t + G_t U_t + E_t))}{\partial \Lambda_{t+1}} \Bigg|_{\substack{\Lambda_{t+1} = \Lambda_{t+1}^\theta \\ X_t = X_t^\theta \\ U_t = U_t^\theta}} \\ &= F_t X_t^\theta + G_t U_t^\theta + E_t = \mathbf{0}. \end{aligned} \quad (\text{A.2a})$$

The costate equation:

$$\begin{aligned} \frac{\partial \bar{H}_t}{\partial X_t^\theta} &= \frac{\partial \text{Tr} (\frac{1}{2} X_t' H_t^{xx} X_t) + \partial \text{Tr} (U_t' H_t^{ux} X_t) + \partial \text{Tr} (H_t^{ex} X_t) + \partial \text{Tr} (\Lambda'_{t+1} F_t X_t)}{\partial X_t} \Bigg|_{\substack{\Lambda_{t+1} = \Lambda_{t+1}^\theta \\ X_t = X_t^\theta \\ U_t = U_t^\theta}} \\ &= H_t^{xx} X_t^\theta + H_t^{xu} U_t^\theta + H_t^{xe} + F_t' \Lambda_{t+1}^\theta = \Lambda_t^\theta. \end{aligned} \quad (\text{A.2b})$$

Input equation:

$$\begin{aligned} \frac{\partial \bar{H}_t}{\partial U_t^\theta} &= \frac{\partial \text{Tr} (\frac{1}{2} U_t' H_t^{uu} U_t) + \partial \text{Tr} (U_t' H_t^{ux} X_t) + \partial \text{Tr} (H_t^{eu} U_t) + \partial \text{Tr} (\Lambda'_{t+1} G_t U_t)}{\partial U_t} \Bigg|_{\substack{\Lambda_{t+1} = \Lambda_{t+1}^\theta \\ X_t = X_t^\theta \\ U_t = U_t^\theta}} \\ &= H_t^{uu} U_t^\theta + H_t^{ux} X_t^\theta + H_t^{ue} + G_t' \Lambda_{t+1}^\theta = \mathbf{0}. \end{aligned} \quad (\text{A.2c})$$

And boundary condition:

$$\Lambda_T^\theta = \frac{\partial \text{Tr} (\frac{1}{2} X_T' H_T^{xx} X_T) + \partial \text{Tr} ((H_T^{xe})' X_T)}{\partial X_T} \Bigg|_{X_T = X_T^\theta} = H_T^{xx} X_T^\theta + H_T^{xe}. \quad (\text{A.2d})$$

Note that in the above derivations, we use the following matrix calculus [45]:

$$\frac{\partial \text{Tr}(AB)}{\partial A} = B', \quad \frac{\partial f(A)}{\partial A'} = \left[\frac{\partial f(A)}{\partial A} \right]', \quad \frac{\partial \text{Tr}(X'HX)}{\partial X} = HX + H'X, \quad (\text{A.3})$$

and the following matrix trace properties:

$$\text{Tr}(A) = \text{Tr}(A'), \quad \text{Tr}(ABC) = \text{Tr}(BCA) = \text{Tr}(CAB), \quad \text{Tr}(A+B) = \text{Tr}(A) + \text{Tr}(B). \quad (\text{A.4})$$

Since the above obtained PMP equations (A.2) are the same with the differential PMP in (13), we thus can conclude that the Pontryagin's Maximum Principle of the auxiliary control system $\bar{\Sigma}(\xi_\theta)$ in (16) is exactly the differential PMP equations (13), and thus (17) holds. This completes the proof. \square

B Proof of Lemma 5.2

Based on Lemma 5.1 and its proof, we know that the PMP of the auxiliary control system, (A.2), is exactly the differential PMP equations (13). Thus below we only look at the differential PMP equations in (A.2). From (A.2c), we solve for U_t^θ :

$$U_t^\theta = -(H_t^{uu})^{-1} (H_t^{ux} X_t^\theta + G_t' \Lambda_{t+1}^\theta + H_t^{ue}). \quad (\text{A.5})$$

By substituting (A.5) into (A.2a) and (A.2b), respectively, and considering the definitions of matrices A_t, R_t, M_t, Q_t and N_t in (18), we have

$$X_{t+1}^\theta = A_t X_t^\theta - R_t \Lambda_{t+1}^\theta + M_t, \quad (\text{A.6})$$

$$\Lambda_t^\theta = Q_t X_t^\theta + A_t' \Lambda_{t+1}^\theta + N_t, \quad (\text{A.7})$$

for $t = 0, 1, \dots, T-1$, and

$$\Lambda_T^\theta = H_T^{xx} X_T^\theta + H_T^{xe}, \quad (\text{A.8})$$

for $t = T$. Next, we prove that there exist matrices P_t and W_t such that

$$\Lambda_t^\theta = P_t X_t^\theta + W_t. \quad (\text{A.9})$$

Proof by induction: (A.8) shows that (A.9) holds for $t = T$ if $P_T = H_T^{xx}$ and $W_T = H_T^{xe}$. Assume (A.9) holds for $t+1$, then by manipulating (A.6) and (A.7), we have

$$\Lambda_t^\theta = \underbrace{(Q_t + A_t'(I + P_{t+1}R_t)^{-1}P_{t+1}A_t)}_{P_t} X_t^\theta + \underbrace{A_t'(I + P_{t+1}R_t)^{-1}(W_{t+1} + P_{t+1}M_t)}_{W_t} + N_t, \quad (\text{A.10})$$

which indicates (A.9) holds for t , if P_t and W_t satisfy (18a) and (18b), respectively. Substituting (A.9) to (A.7) and also considering (A.5) will lead to (19a). (19b) directly results from (A.2a). We complete the proof. \square

C Proof of Discrete-Time Pontryagin's Maximum Principle

We here provide a easy-approach derivation of the discrete-time PMP based on Karush-Kuhn-Tucker (KKT) conditions in non-linear optimization [46]. The original derivation for continuous optimal control systems uses calculus of variation theory, which can be found in [29] and [47].

We view the optimal control system (1) with a fixed θ as a constrained optimization problem, where the objective function is given by $J(\theta)$ and constraints given by the dynamics f . Define the following Lagrangian for this constrained optimization problem:

$$\begin{aligned} L &= J(\theta) + \sum_{t=0}^{T-1} \lambda'_{t+1} (f(x_t, u_t, \theta) - x_{t+1}) \\ &= \sum_{t=0}^{T-1} \left(c_t(x_t, u_t, \theta) + \lambda'_{t+1} (f(x_t, u_t, \theta) - x_{t+1}) \right) + h(x_T, \theta) \\ &= \sum_{t=0}^{T-1} \left(H_t - \lambda'_{t+1} x_{t+1} \right) + h(x_T, \theta), \end{aligned} \quad (\text{A.11})$$

where λ_t is the Lagrange multiplier for the dynamics constraint for $t = 1, 2, \dots, T$, and the third equation above is due to the definition of Hamiltonian in (10). According to the KKT conditions, for the optimal solution $\xi_\theta = \{x_{0:T}^\theta, u_{0:T-1}^\theta\}$, there must exist the multipliers $\lambda_{1:T}^\theta$ (in optimal control they are called costates) such that the following first-order conditions are satisfied:

$$\frac{\partial L}{\partial \lambda_{1:T}^\theta} = \mathbf{0}, \quad \frac{\partial L}{\partial x_{0:T}^\theta} = \mathbf{0}, \quad \frac{\partial L}{\partial u_{0:T-1}^\theta} = \mathbf{0}. \quad (\text{A.12})$$

By extending the above three conditions in (A.12) at each λ_t, x_t and u_t , respectively, and particularly taking care of x_T , we will obtain

$$\mathbf{0} = f(x_t^\theta, u_t^\theta; \theta) - x_{t+1}^\theta, \quad (\text{A.13a})$$

$$\mathbf{0} = \frac{\partial H_t}{\partial x_t^\theta} - \lambda_t^\theta = \frac{\partial c_t}{\partial x_t^\theta} + \frac{\partial f'}{\partial x_t^\theta} \lambda_{t+1}^\theta - \lambda_t^\theta, \quad (\text{A.13b})$$

$$\mathbf{0} = \frac{\partial H_t}{\partial u_t^\theta} = \frac{\partial c_t}{\partial u_t^\theta} + \frac{\partial f'}{\partial u_t^\theta} \lambda_{t+1}^\theta, \quad (\text{A.13c})$$

$$\mathbf{0} = \frac{\partial h}{\partial x_T} - \lambda_T^\theta. \quad (\text{A.13d})$$

respectively, which are exactly the PMP conditions in (11). This completes the proof. \square

D Algorithms Details for Different Learning Modes

Algorithm 2: Solving $\frac{\partial \xi_\theta}{\partial \theta}$ using Auxiliary Control System

Input: The trajectory ξ_θ generated by the system $\Sigma(\theta)$

Compute the coefficient matrices (14) to obtain the auxiliary control system $\bar{\Sigma}(\xi_\theta)$ in (16);

def Auxiliary_Control_System_Solver ($\bar{\Sigma}(\xi_\theta)$): \triangleright implementation of Lemma 5.2

Set $P_T = H_T^{xx}$ and $W_T = H_T^{xe}$;

for $t \leftarrow T$ **to** 0 **by** -1 **do**

 Update P_t and W_t using equation (18) \triangleright backward in time

end

Set $X_0 = \mathbf{0}$;

for $t \leftarrow 0$ **to** T **by** 1 **do**

 Update X_t and U_t using equation (19) \triangleright forward in time

end

Return: $\{X_{0:T}^\theta, U_{0:T-1}^\theta\}$

Return: $\frac{\partial \xi_\theta}{\partial \theta} = \{X_{0:T}^\theta, U_{0:T-1}^\theta\}$

Algorithm 3: PDP Algorithm for IRL/IOC Mode

Data: Expert demonstration $\{\xi^d\}$

Parameterization: The parameterized optimal control system $\Sigma(\theta)$ in (1)

Loss: $L(\xi_\theta, \theta)$ in (4)

Initialization: θ_0 , learning rate $\{\eta_k\}_{k=0,1,\dots}$

for $k = 0, 1, 2, \dots$ **do**

 Solve ξ_{θ_k} from the current optimal control system $\Sigma(\theta_k)$; \triangleright using any OC solver

 Obtain $\frac{\partial \xi_\theta}{\partial \theta} \big|_{\theta_k}$ using Algorithm 2 given ξ_{θ_k} ; \triangleright using Algorithm 2

 Obtain $\frac{\partial L}{\partial \xi} \big|_{\xi_{\theta_k}}$ from the given loss function $L(\xi_\theta, \theta)$;

 Apply the chain rule (9) to obtain $\frac{dL}{d\theta} \big|_{\theta_k}$;

 Update $\theta_{k+1} \leftarrow \theta_k - \eta_k \frac{dL}{d\theta} \big|_{\theta_k}$;

end

Algorithm 4: PDP Algorithm for SysID Mode

Data: Input-state data $\{\xi^o\}$

Parameterization: The parameterized dynamics model $\Sigma(\theta)$ in (5)

Loss: $L(\xi_\theta, \theta)$ in (6)

Initialization: θ_0 , learning rate $\{\eta_k\}_{k=0,1,\dots}$

for $k = 0, 1, 2, \dots$ **do**

 Obtain ξ_{θ_k} by iteratively integrating $\Sigma(\theta_k)$ in (5) for $t = 0, \dots, T - 1$;

 Compute the coefficient matrices (14) to obtain the auxiliary control system $\bar{\Sigma}(\xi_\theta)$ in (20);

 Obtain $\frac{\partial \xi_\theta}{\partial \theta} \big|_{\theta_k}$ by iteratively integrating $\bar{\Sigma}(\xi_{\theta_k})$ in (20) for $t = 0, \dots, T - 1$;

 Obtain $\frac{\partial L}{\partial \xi} \big|_{\xi_{\theta_k}}$ from the given loss function in (6);

 Apply the chain rule (9) to obtain $\frac{dL}{d\theta} \big|_{\theta_k}$;

 Update $\theta_{k+1} \leftarrow \theta_k - \eta_k \frac{dL}{d\theta} \big|_{\theta_k}$;

end

Algorithm 5: PDP Algorithm for Control/Planning Mode

Parameterization: The parameterized-policy system $\Sigma(\theta)$ in (7)

Loss: $L(\xi_\theta, \theta)$ in (8)

Initialization: θ_0 , learning rate $\{\eta_k\}_{k=0,1,\dots}$

for $k = 0, 1, 2, \dots$ **do**

 Obtain ξ_{θ_k} by iteratively integrating $\Sigma(\theta_k)$ in (7) for $t = 0, \dots, T - 1$;

 Compute the coefficient matrices (14) to obtain the auxiliary control system $\bar{\Sigma}(\xi_\theta)$ in (21);

 Obtain $\frac{\partial \xi_\theta}{\partial \theta} \big|_{\theta_k}$ by iteratively integrating $\bar{\Sigma}(\xi_{\theta_k})$ in (21) for $t = 0, \dots, T - 1$;

 Obtain $\frac{\partial L}{\partial \xi} \big|_{\xi_{\theta_k}}$ from the given loss function $L(\xi_\theta, \theta)$ in (8);

 Apply the chain rule (9) to obtain $\frac{dL}{d\theta} \big|_{\theta_k}$;

 Update $\theta_{k+1} \leftarrow \theta_k - \eta_k \frac{dL}{d\theta} \big|_{\theta_k}$;

end

Additional discussion: combining different learning modes. In addition to using different learning modes to solve different types of problems, one can combine different modes in a single learning task. For example, when solving model-based reinforcement learning, one can call SysID Mode to first learn a dynamics model, then use the learned dynamics in Control/Planning Mode to obtain an optimal policy. In problems such as imitation learning, one can first learn a dynamics model using SysID Mode, then use the learned dynamics as the initial guess in IRL/IOC Mode. In forward pass of IOC/IRL Mode, one can call Control/Planning Mode to solve the OC system. For control and planning problems, the loss required in Control/Planning Mode can be learned using IOC/IRL Mode. In MPC-based learning and control applications [48], one can use the general formulation (3) to learn a MPC controller, and then execute the MPC controller by calling Control/Planning Mode.

E Experiment Details

UAV Maneuvering Control on SE(3). In our experiments, we consider UAV maneuvering on SE(3) space (i.e. full position and full attitude space). The equation of motion of an UAV is given by:

$$\begin{aligned} \dot{\mathbf{p}}_I &= \dot{\mathbf{v}}_I, \\ m\dot{\mathbf{v}}_I &= m\mathbf{g}_I + \mathbf{F}_I, \\ \dot{\mathbf{q}}_{B/I} &= \frac{1}{2}\Omega(\boldsymbol{\omega}_B)\mathbf{q}_{B/I}, \\ J_B\dot{\boldsymbol{\omega}}_B &= \mathbf{M}_B - \boldsymbol{\omega} \times J_B\boldsymbol{\omega}_B. \end{aligned} \tag{A.14}$$

Here, the subscriptions B and I denote that a quantity is expressed in the body frame and inertial (world) frame, respectively; m is the mass of the UAV; $\mathbf{p} \in \mathbb{R}^3$ and $\mathbf{v} \in \mathbb{R}^3$ are the position and velocity vector of the UAV; $J_B \in \mathbb{R}^{3 \times 3}$ is the moment of inertia of the UAV with respect to body frame; $\boldsymbol{\omega}_B \in \mathbb{R}^3$ is the angular velocity of the UAV; $\mathbf{q}_{B/I} \in \mathbb{R}^4$ is the unit quaternion [49] describing the attitude of UAV with respect to the inertial frame; $\Omega(\boldsymbol{\omega}_B)$ is defined as

$$\Omega(\boldsymbol{\omega}_B) = \begin{bmatrix} 0 & -\omega_x & -\omega_y & -\omega_z \\ \omega_x & 0 & \omega_z & -\omega_y \\ \omega_y & -\omega_z & 0 & \omega_x \\ \omega_z & \omega_y & -\omega_x & 0 \end{bmatrix}; \tag{A.15}$$

$\mathbf{M}_B \in \mathbb{R}^3$ is the torque applied to the UAV; and $\mathbf{F}_I \in \mathbb{R}^3$ is the force vector applied to the UAV center of mass. The total force magnitude $f \in \mathbb{R}$ (along the z-axis of the body frame) and torque $\mathbf{M}_B = [M_x, M_y, M_z]$ are generated by thrust $[T_1, T_2, T_3, T_4]$ of the four UAV rotating propellers, which can be written as

$$\begin{bmatrix} f \\ M_x \\ M_y \\ M_z \end{bmatrix} = \begin{bmatrix} 1 & 1 & 1 & 1 \\ 0 & -l_w/2 & 0 & l_w/2 \\ -l_w/2 & 0 & l_w/2 & 0 \\ c & -c & c & -c \end{bmatrix} \begin{bmatrix} T_1 \\ T_2 \\ T_3 \\ T_4 \end{bmatrix}, \tag{A.16}$$

with l_w being the wing length of the UAV and c being a fixed constant.

We define the state vector of the UAV

$$\mathbf{x} = [\mathbf{p}' \quad \mathbf{v}' \quad \mathbf{q}' \quad \boldsymbol{\omega}']' \in \mathbb{R}^{13}. \quad (\text{A.17})$$

and define the control input

$$\mathbf{u} = [T_1 \quad T_2 \quad T_3 \quad T_4]' \in \mathbb{R}^4. \quad (\text{A.18})$$

In design of the control objective function, to achieve SE(3) maneuvering control performance, we need to carefully design the attitude error. As used in [50], we define the attitude error between the UAV's current attitude \mathbf{q} and the goal attitude \mathbf{q}_g as

$$e(\mathbf{q}, \mathbf{q}_g) = \frac{1}{2} \text{Tr}(I - R'(\mathbf{q}_g)R(\mathbf{q})), \quad (\text{A.19})$$

where $R \in \mathbb{R}^{3 \times 3}(\mathbf{q})$ are the direction cosine matrix directly corresponding to the quaternion \mathbf{q} (see [49] for more details). Other error term in the control objective is the squared distance to the respective goal, that is,

$$e(\mathbf{p}, \mathbf{p}_g) = \|\mathbf{p} - \mathbf{p}_g\|^2, \quad e(\mathbf{v}, \mathbf{v}_g) = \|\mathbf{v} - \mathbf{v}_g\|^2, \quad e(\boldsymbol{\omega}, \boldsymbol{\omega}_g) = \|\boldsymbol{\omega} - \boldsymbol{\omega}_g\|^2. \quad (\text{A.20})$$

Multi-link Robot Arm. The dynamics of N -link robot arm can be found in [51, p. 171], where the system state is $\mathbf{x} = [\mathbf{q}, \dot{\mathbf{q}}]$ with $\mathbf{q} \in \mathbb{R}^N$ being the vector of angles of N joints and $\dot{\mathbf{q}}$ being the vector of angular velocity of N joints, and the input $\mathbf{u} \in \mathbb{R}^N$ is the vector of torques applied to each joint.

The continuous-time dynamics of all experiment systems in Table 2 are discretized using the Euler method: $\mathbf{x}_{t+1} = \mathbf{x}_t + \Delta \cdot \mathbf{f}(\mathbf{x}_t, \mathbf{u}_t)$ with the discretization interval $\Delta = 0.05\text{s}$ or $\Delta = 0.1\text{s}$.

Experiments of Imitation Learning. In the imitation learning experiment, the dataset of expert demonstrations $\{\boldsymbol{\xi}^d\}$ is generated by solving the expert's optimal control system with the expert's dynamics and control objective parameter $\boldsymbol{\theta}^* = \{\boldsymbol{\theta}_{\text{dyn}}^*, \boldsymbol{\theta}_{\text{dyn}}^*\}$ known. We generate a total number of five trajectories, where different trajectory $\boldsymbol{\xi}^d = \{\mathbf{x}_{0:T}^d, \mathbf{u}_{0:T-1}^d\}$ has different initial condition \mathbf{x}_0 and time horizon T (the horizon T ranges from 40 to 50).

We choose the inverse KKT method [39] for comparison because it is suitable for learning objective functions for high-dimensional continuous-space systems. We adapt the inverse KKT method in [39], and define the KKT loss as the norm-2 violation of the KKT condition (A.12) by the demonstration data $\boldsymbol{\xi}^d$:

$$\min_{\boldsymbol{\theta}, \boldsymbol{\lambda}_{1:T}} \left(\left\| \frac{\partial L}{\partial \mathbf{x}_{0:T}}(\mathbf{x}_{0:T}^d, \mathbf{u}_{0:T-1}^d) \right\|^2 + \left\| \frac{\partial L}{\partial \mathbf{u}_{0:T-1}}(\mathbf{x}_{0:T}^d, \mathbf{u}_{0:T-1}^d) \right\|^2 \right), \quad (\text{A.21})$$

where $\frac{\partial L}{\partial \mathbf{x}_{0:T}}(\cdot)$ and $\frac{\partial L}{\partial \mathbf{u}_{0:T-1}}(\cdot)$ are defined in (A.12) and $\boldsymbol{\theta} = \{\boldsymbol{\theta}_{\text{dyn}}, \boldsymbol{\theta}_{\text{dyn}}\}$. We minimize such KKT-loss (i.e. the optimality violation) with respect to the unknown $\boldsymbol{\theta}$ and the costate variables $\boldsymbol{\lambda}_{1:T}$.

Note that to illustrate the inverse-KKT results in Fig. 3, we plot the imitation loss $L(\boldsymbol{\xi}_\theta, \boldsymbol{\theta}) = \mathbb{E}_{\boldsymbol{\xi}^d} \|\boldsymbol{\xi}^d - \boldsymbol{\xi}_\theta\|^2$ instead of the KKT loss (A.21), and this is because we want to guarantee the comparison item is consistent across different methods. Thus for each iteration k of minimizing the KKT loss (A.21), we use its current parameter $\boldsymbol{\theta}_k$ to generate the system trajectory $\boldsymbol{\xi}_{\boldsymbol{\theta}_k}$ and compute the imitation loss.

For the neural policy imitation learning (similar to [52]), we directly learn a neural-network control policy $\mathbf{u} = \boldsymbol{\pi}_\theta(\mathbf{x})$ from the dataset using supervised learning, that is

$$\min_{\boldsymbol{\theta}} \sum_{t=0}^{T-1} \|\mathbf{u}_t^d - \boldsymbol{\pi}_\theta(\mathbf{x}_t^d)\|^2. \quad (\text{A.22})$$

In Appendix Fig. 6, we show more detailed results of imitation loss versus iteration for the three systems (cart-pole, robot arm, and UAV). On each system, we run five trials for all methods with random initial guess, and the learning rate for all methods is set as $\eta = 10^{-4}$. In Appendix Fig. 9,

we validate the learned models (i.e., learned dynamics and learned control objective) by performing motion planning of each system in unseen settings. Specifically, we set each system with new initial state \mathbf{x}_0 and horizon T and plan the control trajectory using the learned models; and we also show the corresponding true trajectory of the expert. Please visit link <https://youtu.be/awVNiCIJCfs> for video demos of the above results.

Experiments of System Identification. In the system identification experiment, we collect a total number of five trajectories from systems with dynamics known, wherein different trajectory $\xi^o = \{\mathbf{x}_{0:T}^o, \mathbf{u}_{0:T-1}\}$ has different initial condition \mathbf{x}_0 and horizon T (T ranges from 10 to 20), with random inputs $\mathbf{u}_{0:T-1}$.

The DMDc method [43], which can be viewed as a variant of Koopman theory [6], estimates a linear dynamics model

$$\mathbf{x}_{t+1} = A\mathbf{x}_t + B\mathbf{u}_t, \quad (\text{A.23})$$

using the following least square regression

$$\min_{A,B} \sum_{t=0}^{T-1} \|\mathbf{x}_{t+1}^o - A\mathbf{x}_t^o - B\mathbf{u}_t\|^2. \quad (\text{A.24})$$

For the neural network baseline, we use a neural network $\mathbf{f}_\theta(\mathbf{x}, \mathbf{u})$ to represent the system dynamics, where the input of the network is state and control vectors, and output is the state of next step. We train the neural network by minimizing the following residual

$$\min_{\theta} \sum_{t=0}^{T-1} \|\mathbf{x}_{t+1}^o - \mathbf{f}_\theta(\mathbf{x}_t^o, \mathbf{u}_t)\|^2. \quad (\text{A.25})$$

In Appendix Fig. 7, we show more detailed results of SysID loss versus iteration for the three systems (cart-pole, robot arm, and UAV). On each system, we run five trials with random initial guess, and we set the learning rate as $\eta = 10^{-4}$ for all methods. In Appendix Fig. 10, we use the learned dynamics model to perform motion prediction of each system in unactuated conditions, in order to validate the effectiveness/correctness of the learned dynamics models. Please visit the link <https://youtu.be/PAyBZjDD60Y> for video demos of the above results.

Experiments of Optimal Control. In the optimal control experiment, we parameterize the control policy $\mathbf{u}_t = \mathbf{u}(t, \mathbf{x}_t, \boldsymbol{\theta})$ as N -degree Lagrange polynomial [53] with $N + 1$ collocation/pivot points evenly populated over the time horizon, that is, $\{(t_0, \mathbf{u}_0), (t_1, \mathbf{u}_1), \dots, (t_N, \mathbf{u}_N)\}$ with $t_i = iT/N$, $i = 0, \dots, N$. The analytical form of the parameterized policy is

$$\mathbf{u}(t) = \sum_{i=0}^N \mathbf{u}_i b_i(t) \quad \text{with} \quad b_i(t) = \prod_{0 \leq j \leq N, j \neq i} \frac{t - t_j}{t_i - t_j}. \quad (\text{A.26})$$

Here, $b_i(t)$ is called Lagrange basis, and the tunable parameter vector is

$$\boldsymbol{\theta} = [\mathbf{u}_0, \dots, \mathbf{u}_N]' \in \mathbb{R}^{m(N+1)} \quad (\text{A.27})$$

We choose the above time-dependent parameterization due to the following reasons. First, a finite-horizon optimal control system typically correspond to a time-varying optimal policy; in other words, in finite-horizon optimal control, the optimal control input \mathbf{u}_t depends not only on the current system state \mathbf{x}_t but also on the time step t it encounters. Second, this polynomial parameterization has been normally used in some trajectory optimization method such as [31, 54]. In optimal control/planning experiments, we here use the time horizon T ranging from 20 to 40.

In Appendix Fig. 8, we show the detailed results of the control loss (i.e. the value of control objective) versus iterations for three systems (cart-pole, robot arm, and UAV). For each system, we run five trials with random initial parameter for the PDP and random nominal trajectory for iLQR, and we set the learning rate $\eta = 10^{-4}$ for both the PDP and iLQR methods. For reference, we also plot the ground-truth minimal control loss solved by an OC solver [44]. In Appendix Fig. 11, we illustrate the final (converged) control trajectory learned by the PDP and iLQR, and also plot the ground-truth optimal control trajectory solved using the OC solver [44]. Please visit the link <https://youtu.be/KTw6TAigfPY> for video demos of the above results.

Please find the separate experiment for 6 DoF rocket powered landing in Appendix I.

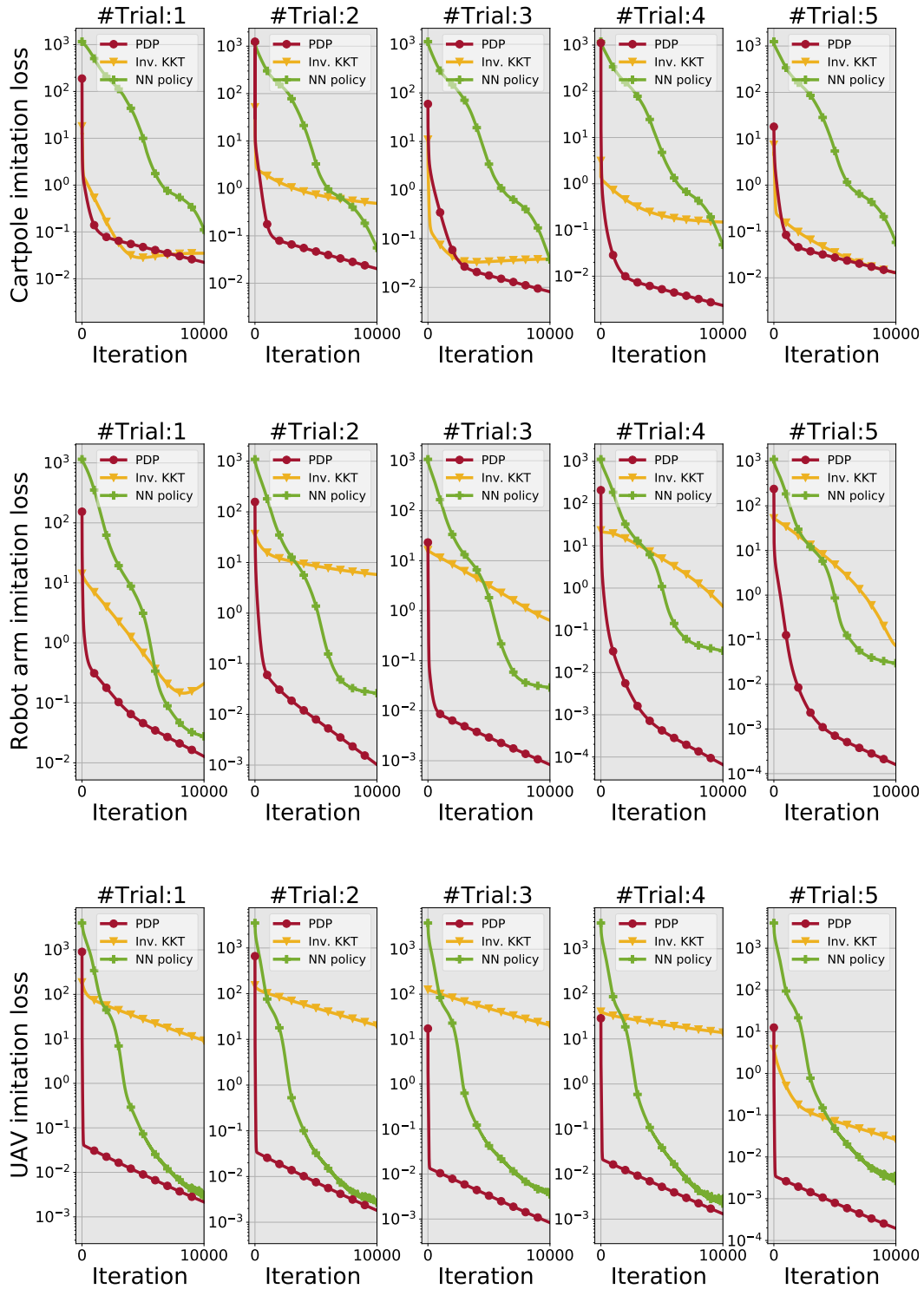


Figure 6: Experiments for PDP IRL/IOC Mode: imitation loss versus iteration. For each system, we run five trials starting with random initial guess θ_0 , and the learning rate is $\eta = 10^{-4}$ for all methods. The results show a significant advantage of the PDP over the neural policy imitation/cloning and inverse-KKT [39] in terms of lower training loss and faster convergence speed. Please see Appendix Fig. 9 for validation. Please find the video demos at link <https://youtu.be/awVNiCfCs>.

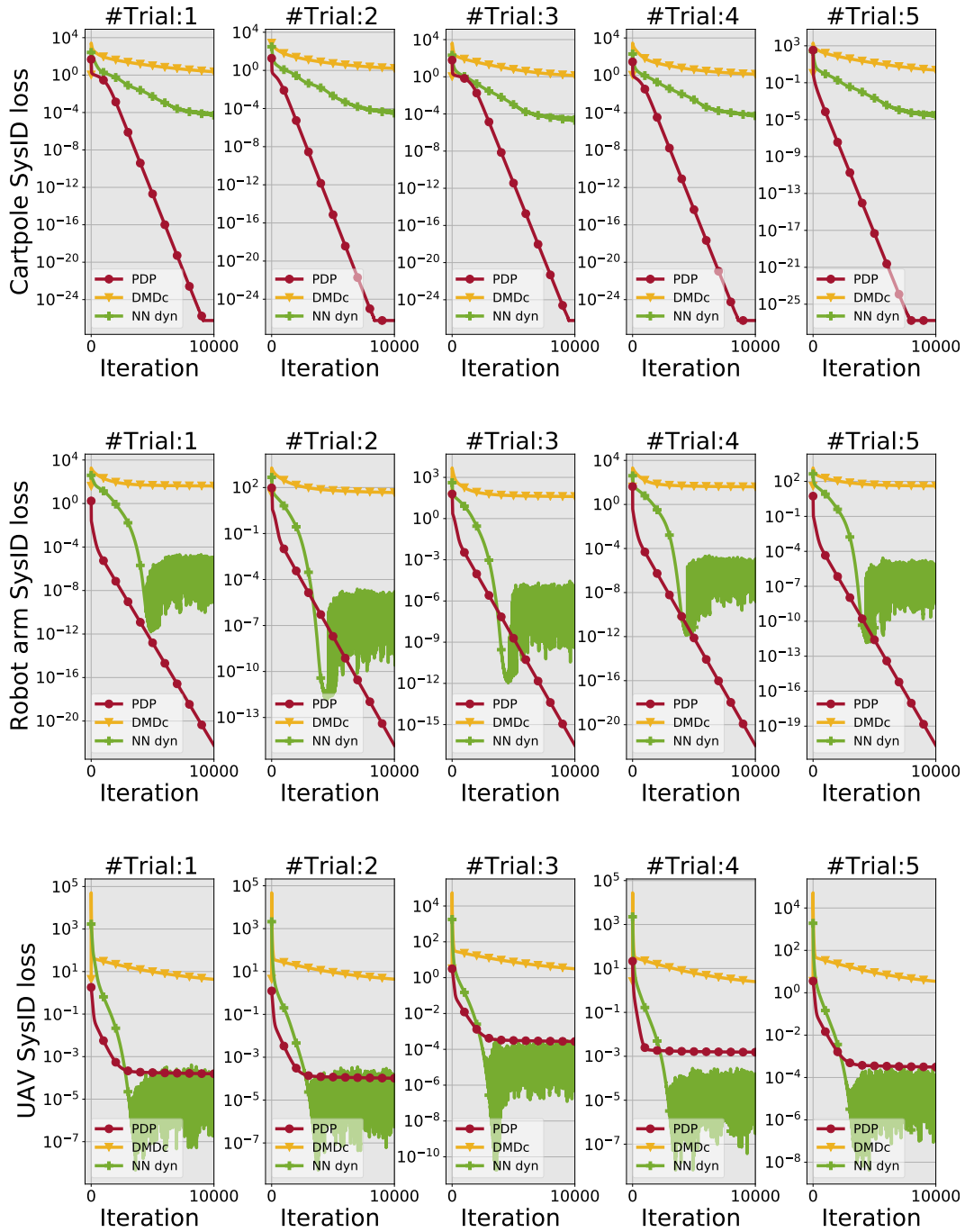


Figure 7: Experiments for PDP SysID Mode: SysID loss versus iteration. For each system, we run five trials with random initial guess θ_0 , and set the learning rate $\eta = 10^{-4}$ for all methods. The results show a significant advantage of the PDP over neural-network learning and DMDc in terms of lower training loss and faster convergence speed. Please see Appendix Fig. 10 for validation. Please find the video demos at link <https://youtu.be/PAYBZjDD60Y>.

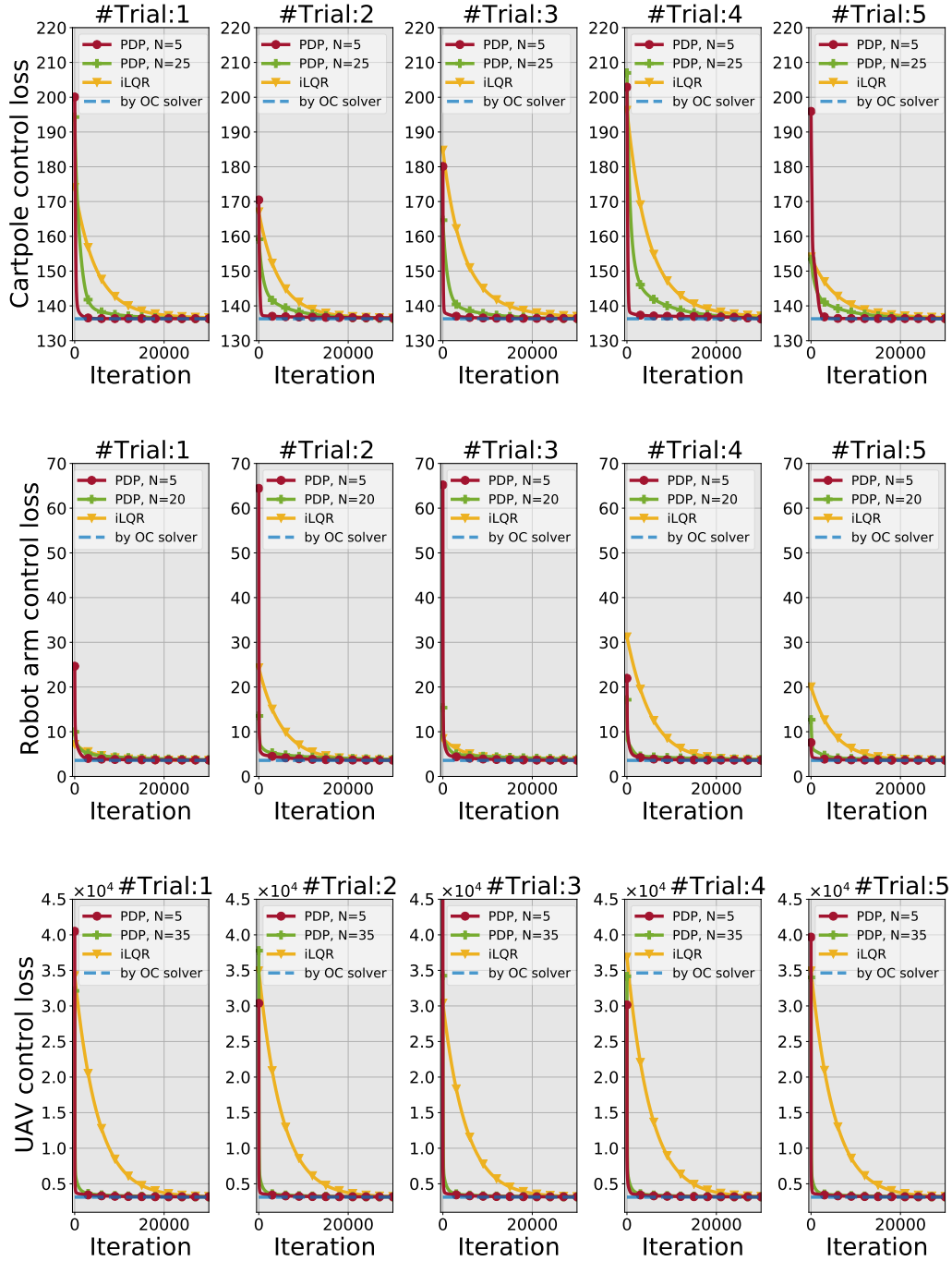


Figure 8: Experiments for PDP Control/Planning Mode: control loss (cost function value) versus iteration. For each system, we run five trials with random initial θ_0 for the PDP and random nominal trajectories for iLQR, and also plot the true minimal control loss solved by an OC solver [44], and the learning rate is 10^{-4} for all methods. The results show the significant advantage of the PDP over iLQR in terms of faster convergence speed. Please see Appendix Fig. 11 for validation and discussions. Please find the video demos at link <https://youtu.be/KTw6TAigfPY>.

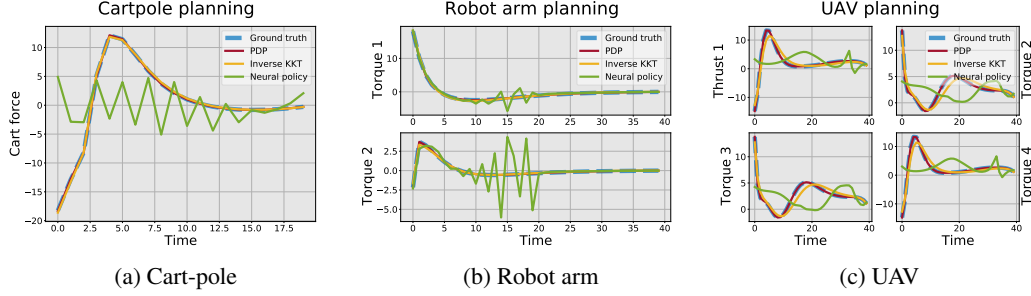


Figure 9: Validation for the imitation learning experiment in Appendix Fig. 6: we preform motion planning for each system in unseen conditions (new initial condition and new time horizon) using the learned models. Results show that compared to the neural policy imitation/cloning and inverse KKT [39], the PDP result can accurately plan the expert’s trajectory in novel settings. This indicates PDP can accurately learn the dynamics and control objective, and has the better generality than the other two.

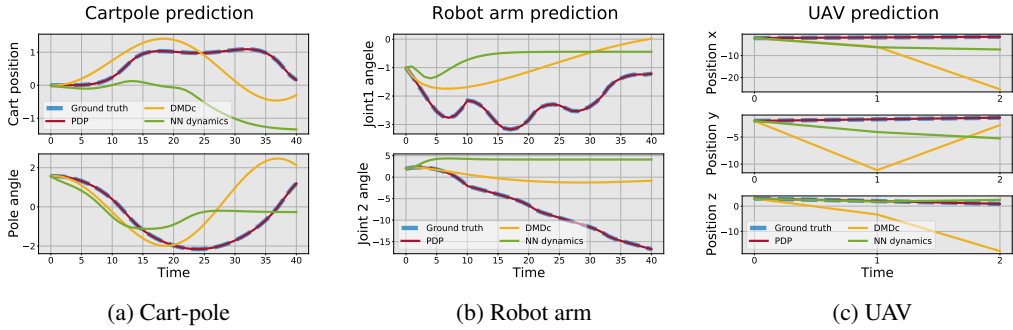


Figure 10: Validation for the system identification experiment in Appendix Fig. 7: motion prediction of each system in un-actuated conditions using the learned dynamics. Results show that compared to neural-network dynamics training and DMDC, the PDP can accurately predict the motion trajectory of each systems. This indicates the effectiveness of the PDP in identifying dynamics models.

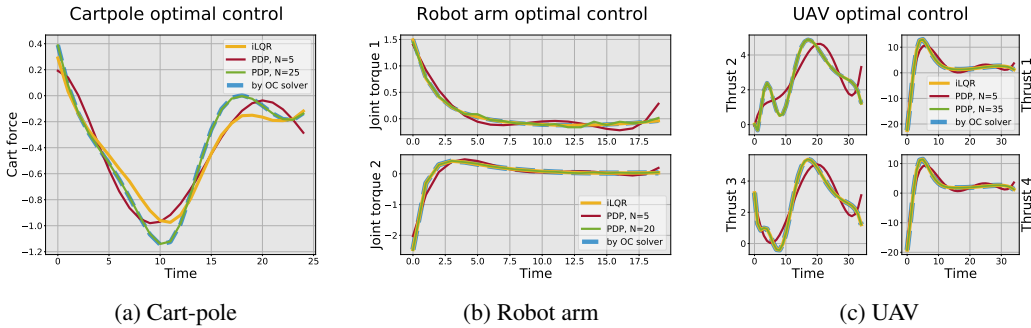


Figure 11: Validation for the optimal control experiment in Appendix Fig. 8: the learned control trajectory using PDP and iLQR, and also a ground-truth optimal trajectory solved by an OC solver [44]. The results shows that PDP method can successfully learn a policy such that its trajectory very close to the ground truth optimal trajectory. We also observe that accuracy of the learned trajectory depends on choice of the policy parameterization (i.e., expressive power): for example, the use of polynomial policy of a higher degree N results in a trajectory closer to the optimal one than the use of a lower degree. iLQR is generally able to achieve high-accurate solutions because it directly optimizes the loss function with respect to the control trajectory, but this comes at the cost of high computation and slower convergence. Note that in (a), iLQR also shows a low accuracy.

F Comparison with Other Learning Frameworks

We discuss the difference of the PDP framework from existing end-to-end learning frameworks, and present the comparison of algorithm complexity.

Differentiable MPC. [48] develops an end-to-end differentiable MPC framework to jointly learn the system dynamics model and control objective function of an optimal control system. In forward pass, it first uses iLQR [28] to solve the optimal control system and find a fixed point, and approximate the optimal control system by a LQR system at the fixed point. In backward pass, the gradient is obtain by differentiating the LQR approximation. This process, however, may have two drawbacks: first, since the differentiation in backward pass is conducted on the LQR approximation instead of on the original system, the obtained gradient thus may not be accurate due to the discrepancy of the approximation; and second, the gradient of the LQR approximation is computed via solving a large linear equation, whose size is linear to the horizon of the control system, and this may cause huge computational cost when handling the system of longer time horizon.

Compared to differentiable MPC, the first advantage of the PDP framework is that the differentiation in backward pass of PDP is directly performed on the parameterized optimal control system (by differentiating PMP). Second, we develop the auxiliary control system in backward pass of PDP, whose trajectory output is exactly the gradient of the system trajectory. The gradient then is iteratively solved from the auxiliary control system using Lemma 5.2 (Algorithm 2). Those proposed techniques enables the PDP framework to have significant advantage in efficiency over differentiable MPC. To illustrate this, we have compare the algorithm complexity in Table 3 and provide a comparison experiment in Fig. 12.

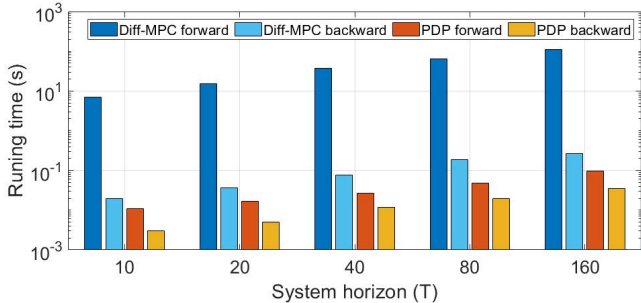


Figure 12: Runtime (per iteration) comparison between the proposed PDP and differentiable MPC [48] for different time horizons of a pendulum optimal control system. Note that y-axis is log-scale, and the runtime is averaged over 100 iterations. Both methods are implemented in Python and run on the same machine using CPUs. The results show that the PDP runs 1000x faster than differentiable MPC.

Path Integral Network. [55] and [56] develop a differentiable end-to-end framework to learn path-integral optimal control systems. Path-integral optimal control systems [57] however are a limited category of optimal control systems, where the dynamics is affine in control inputs and the control objective function is quadratic in control. More importantly, this path integral network is essentially an ‘unrolling’ method, which means that the forward pass of solving optimal control is extended as a graph of multiple steps of applying gradient descent, and the solution of the optimal control system is considered as the output of the final step of gradient descent. Although the advantage of this unrolling (gradient descent) computational graph is that it can immediately take advantage of the automatic differentiation technique such as TensorFlow [58] to obtain the gradient in backpropagation, its drawback is however obvious: the framework is both memory- and computationally- expensive because it needs to store and traverse all intermediate results of the gradient descent process; furthermore, there is a conflict between computational complexity and accuracy in the forward pass. We have provided its complexity analysis in Table 3.

Universal Planning Network. In [59], the authors develop an end-to-end imitation learning framework consisting of two layers: the inner layer is a planner, which is formulated as an optimal control system in latent space and is solved by gradient descent, and an outer layer to minimize the imitation

loss between the output of inner layer and expert demonstrations. However, the development of this framework is also based on the ‘unrolling’ strategy. Specifically, the inner planning layer based on gradient descent is considered as a large computation graph, which chains together the sub-graphs of each iteration of gradient descent. In backward pass, the gradient derived from the outer layer back-propagates through the entire computation graph. Again, this unrolled learning strategy will incur huge memory and computation costs in implementation. Please find its complexity analysis in Table 3.

Different from the above ‘unrolling’ learning methods [55, 56, 59, 60], the proposed PDP method handles the learning of optimal control systems in a ‘direct and compact’ way. Specifically, in forward pass, PDP only obtains and stores the final solution of an optimal control system and does not care about the (intermediate) process of how such solution is obtained. Thus, the forward pass of the PDP accepts any external optimal control solver such as efficient CasADi [44]. Using the solution in forward pass, the PDP then automatically builds the auxiliary control system, based on which, the gradient is efficiently (iteratively) solved in backward pass. Such features guarantee that the complexity of the PDP framework is only linearly scaled up to the time horizon of the optimal control system, which is significantly efficient than the above ‘unrolling’ learning methods (please find the comparison in Table 3). In Appendix G, we will present the detailed complexity analysis of the PDP.

Table 3: Complexity comparison for different end-to-end learning frameworks

Learning frameworks	Forward pass		Backward pass	
	Method and accuracy	Complexity (linear to)	Method	Complexity (linear to)
PI-Net [55]	N -step unrolled graph by gradient descent; accuracy depends on N	computation: NT memory: NT	Back-propagation over the unrolled graph	computation: NT memory: NT
UPN [59]	N -step unrolled graph by gradient descent; accuracy depends on N	computation: NT memory: NT	Back-propagation over the unrolled graph	computation: NT memory: NT
Diff-MPC [48]	iLQR finds fixed points; can achieve any accuracy	computation: — memory: T	Differentiate the LQR approximation and solve linear equations	computation: T^2 memory: T^2
PDP	Accept any OC solver; can achieve any accuracy	computation: —, memory: T	Auxiliary control system	computation: T , memory: T

*Here T denotes the time horizon of a control system;

G Complexity and Scalability Analysis of the PDP

We consider the algorithms of different learning modes of the PDP (see Appendix D), and suppose the time horizon of the parameterized system $\Sigma(\theta)$ is T .

IRL/IOC Mode (Algorithm 3): in forward pass, the PDP needs to obtain and store the optimal trajectory ξ_θ of the optimal control system $\Sigma(\theta)$ in (1), and this optimal trajectory can be solved by any (external) optimal control solver. In backward pass, the PDP first uses ξ_θ to build the auxiliary control system $\bar{\Sigma}(\xi_\theta)$ in (16) and then computes $\frac{\partial \xi_\theta}{\partial \theta}$ by Lemma 5.2, which takes $2T$ steps.

SysID Mode (Algorithm 4): in forward pass, the PDP needs to obtain and store the trajectory ξ_θ of the original dynamics system $\Sigma(\theta)$ in (5). Such trajectory is simply a result of iterative integration of (5), which takes T steps. In backward pass, the PDP first uses ξ_θ to build the auxiliary control system $\bar{\Sigma}(\xi_\theta)$ in (20) and then computes $\frac{\partial \xi_\theta}{\partial \theta}$ by iterative integration of (20), which takes T steps.

Control/Planning Mode (Algorithm 5): in forward pass, the PDP needs to obtain and store the trajectory ξ_θ of the controlled system $\Sigma(\theta)$ in (7). Such trajectory is simply a result of iterative integration of (7), which takes T steps. In backward pass, the PDP first uses ξ_θ to build an auxiliary control system $\bar{\Sigma}(\xi_\theta)$ in (21) and then computes $\frac{\partial \xi_\theta}{\partial \theta}$ by iterative integration of (21), which takes T steps.

Therefore, we can summarize that the memory- and computational- complexity for the PDP framework is only linear to the time horizon T of the parameterized system $\Sigma(\theta)$. This is significantly advantageous compared to existing end-to-end learning framework, as summarized in Table 3.

H Limitation of the PDP Framework

The PDP methodology provides a systematic framework for learning objective functions, control policies, or dynamics of a system. For SysID and Control/Planning Modes, we need to notice that the PDP in fact is a first-order method (it only uses the *first-order differentiation of dynamics* and loss (cost) function). This is in contrast to the high-order methods, such as iLQR which can be conceptually considered as one-and-half order because it uses the second-order differentiation of value function and first-order differentiation of dynamics, and DDP which is a second-order method as it uses the second-order differentiation of both value cost function and cost function. As empirically shown in the optimal control experiment in Appendix Fig. 8, although the PDP Control/Planning Mode shows advantage of much faster convergence over iLQR, it may not have the lower training loss than iLQR, as shown in Appendix Fig. 11b, (this of course also depends on the parameterization of the policy). See more empirical comparisons between first- or second- learning techniques in [61]

We also want to point out an empirical observation to the PDP methods. Let us assume the obtained trajectory ξ_θ of the original control system $\Sigma(\theta)$ in forward pass is not accurate due to, for example, computational error, which may come from, say, a bad OC solver or inaccurate integrator. As the auxiliary control system $\bar{\Sigma}(\xi_\theta)$ is built on ξ_θ , the gradient $\frac{\partial \xi_\theta}{\partial \theta}$ produced by the auxiliary control system also has the discrepancy from true value. However, we experimentally observe that the gradient is also valid in terms of decreasing the loss, but the final training loss has the error of a level that is nearly proportional to the trajectory error in the forward pass.

I PDP to Solve 6-DoF Rocket Powered Landing Problems

We next demonstrate the capability of the PDP in solving the more challenging 6-DoF rocket powered landing problem. Using the rocket powered landing system, we test the three learning modes of the PDP, respectively.

We here omit the description of mechanics modeling of the 6-DoF powered rocket system, and refer the reader to Page 5 in [62] for the rigid body dynamics model of a rocket system (the notations and coordinates used below are consistent with the ones in [62]). The state variable of the rocket system is defined as

$$\mathbf{x} = [m \quad \mathbf{r}'_{\mathcal{I}} \quad \mathbf{v}'_{\mathcal{I}} \quad \mathbf{q}'_{\mathcal{B}/\mathcal{I}} \quad \boldsymbol{\omega}'_{\mathcal{B}}]' \in \mathbb{R}^{14}, \quad (\text{A.28})$$

where $m \in \mathbb{R}$ is the mass of the rocket; $\mathbf{r}_{\mathcal{I}} \in \mathbb{R}^3$ and $\mathbf{v}_{\mathcal{I}} \in \mathbb{R}^3$ are the position and velocity of the rocket (center of mass) in the inertially-fixed Up-East-North coordinate frame; $\mathbf{q}_{\mathcal{B}/\mathcal{I}} \in \mathbb{R}^4$ is the unit quaternion denoting the attitude of rocket body frame with respect to the inertial frame (also see the description in the UAV dynamics in Appendix E); and $\boldsymbol{\omega}_{\mathcal{B}} \in \mathbb{R}^3$ is the angular velocity of the rocket expressed in the rocket body frame. In our simulation, we only focus on the final descending phase before landing, and we assume the mass depletion in such a short phase is very slow and thus $\dot{m} \approx 0$. We define the control input of the rocket, which is the thrust force vector

$$\mathbf{u} = \mathbf{T}_{\mathcal{B}} = [T_x, T_y, T_z]' \in \mathbb{R}^3, \quad (\text{A.29})$$

acting on the gimbal point of the engine (situated at the tail of the rocket) and is expressed in the body frame. Note that the relationship between the total torque $\mathbf{M}_{\mathcal{B}}$ applied to the rocket and the thrust force vector $\mathbf{T}_{\mathcal{B}}$ is $\mathbf{M}_{\mathcal{B}} = \mathbf{r}_{\mathcal{I},\mathcal{B}} \times \mathbf{T}_{\mathcal{B}}$, with $\mathbf{r}_{\mathcal{I},\mathcal{B}} \in \mathbb{R}^3$ being constant position vector from the center-of-mass to the gimbal point of the engine. The continuous dynamics is discretized using the Euler method: $\mathbf{x}_{t+1} = \mathbf{x}_t + \Delta \cdot \mathbf{f}(\mathbf{x}_t, \mathbf{u}_t)$ with the discretization interval $\Delta = 0.1\text{s}$.

For the rocket control system, the vector of unknown parameters of the dynamics, $\boldsymbol{\theta}_{\text{dyn}}$, includes the initial mass of the rocket m_0 , and the moment of inertia of the rocket $\mathbf{J}_{\mathcal{B}} \in \mathbb{R}^{3 \times 3}$, and the full length of the rocket ℓ , thus,

$$\boldsymbol{\theta}_{\text{dyn}} = \{m_0, \mathbf{J}_{\mathcal{B}}, \ell\} \in \mathbb{R}^8. \quad (\text{A.30})$$

For the control objective function, as shown in Table 2, we consider a weighted combination of the following aspects:

- distance cost of the rocket position from the target position, corresponding to weight w_1 ;
- distance cost of the rocket velocity from the target velocity, corresponding to weight w_2 ;
- penalty of the excessive title angle of the rocket, corresponding to weight w_3 ;

- penalty of the side effects of the thrust vector, corresponding to weight w_4 ;
- penalty of the total fuel cost, corresponding to weighted w_5 .

So the parameter vector of the control objective function, θ_{obj} , is

$$\theta_{\text{obj}} = [w_1, w_2, w_3, w_4, w_5]' \in \mathbb{R}^5. \quad (\text{A.31})$$

In sum, the overall parameter for the 6-DoF rocket powered landing control system is

$$\theta = \{\theta_{\text{dyn}}, \theta_{\text{obj}}\} \in \mathbb{R}^{13}. \quad (\text{A.32})$$

Imitation Learning. We apply the IRL/IOC Mode of the PDP to solve for imitation learning of the 6-DoF rocket powered landing. The experiment process is similar to the experiments in Appendix E, where we collect five trajectories from an expert system with dynamics and control objective function both known (different trajectories have different time horizons T ranging from 40 to 50 and different initial state conditions). Here we minimize imitation loss $L(\xi_\theta, \theta) = \mathbb{E}_{\xi^d} \|\xi^d - \xi_\theta\|^2$ over the parameter of dynamics and control objective, θ in (A.32). The learning rate is set to $\eta = 10^{-4}$, and we run five trials with random initial parameter guess θ_0 . The imitation loss $L(\xi_\theta, \theta)$ versus iteration is plotted in Appendix Fig. 13a. To validate the learned model (the learned dynamics and the learned objective function), we use the learned model to perform motion planning of rocket powered landing in unseen settings (here we use new initial condition and new time horizon). The planing results are plotted in Appendix Fig. 13b, where we also plot the ground truth planning for comparison. Please find the video demos at link <https://youtu.be/4RxDLxUcMp4>.

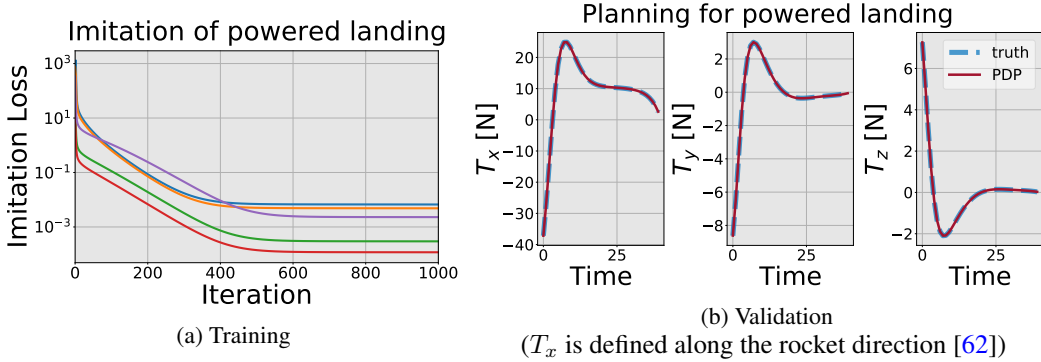


Figure 13: (a) Training process for imitation learning of 6-DoF rocket powered landing: the imitation loss versus iteration; here we have performed five trials (labeled by different colors) with random initial parameter guess. (b) Validation: we use the learned model (dynamics and control objective function) to perform motion planning of the rocket powered landing in unseen settings (i.e. given new initial state condition and new time horizon requirement); here we also plot the ground-truth motion planning of the expert for reference. The results in (a) and (b) show that the PDP can accurately learn the dynamics and control objective function from demonstrations, and have good generalizability to novel situations. Please find the video demos at link <https://youtu.be/4RxDLxUcMp4>.

System Identification. We apply the SysID Mode of the PDP to identify the dynamics parameter θ_{dyn} of the rocket. The experiment process is similar to the experiments in Appendix E, where we collect five trajectories with different initial state conditions, time horizons (T ranges from 10 to 20), and control inputs. We minimize the SysID loss $L(\xi_\theta, \theta) = \mathbb{E}_{\xi^o} \|\xi^o - \xi_\theta\|^2$ over θ_{dyn} in (A.32). The learning rate is set to $\eta = 10^{-4}$, and we run five trials with random initial parameter guess for θ_{dyn} . The SysID loss $L(\xi_\theta, \theta)$ versus iteration is plotted in Appendix Fig. 14a. To validate the learned dynamics, we use it to predict the motion of rocket given a new sequence of control inputs. The prediction results are plotted in Appendix Fig. 14b, where we also plot the ground truth motion (where we know the exact dynamics) for reference.

Optimal Powered Landing Control. We apply the Control/Planning Mode of the PDP to find the optimal control policy for the 6-DoF rocket to perform a successful powered landing.

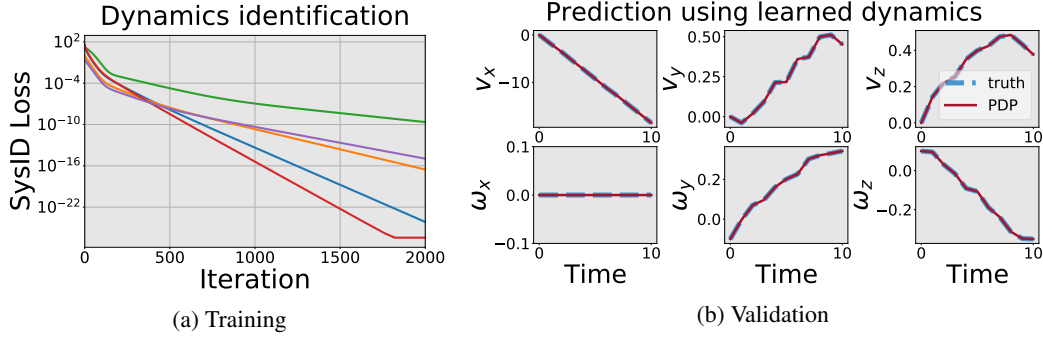


Figure 14: (a) Training process for identification of rocket dynamics: SysID loss versus iteration; here we have performed five trials (labeled by different colors) with random initial parameter guess. (b) Validation: we use the learned dynamics model to perform motion prediction of the rocket given a new control sequence; here we also plot the ground-truth motion (where we know the exact dynamics). The results in (a) and (b) show that the PDP can accurately identify the dynamics model of the rocket.

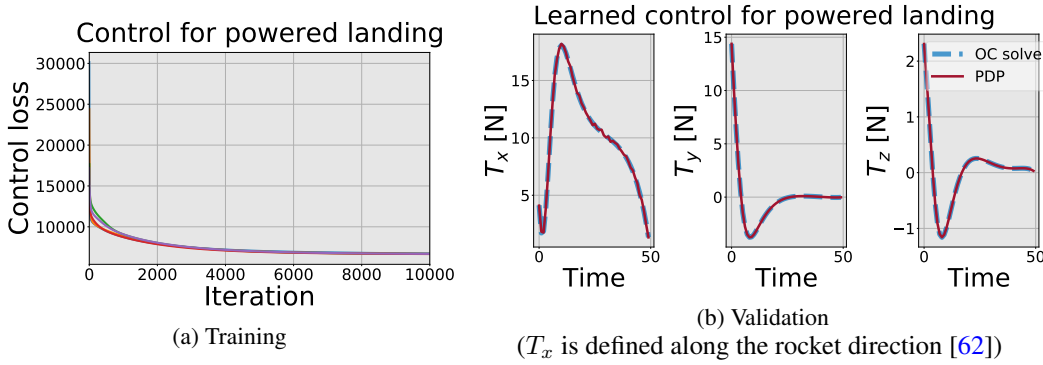


Figure 15: (a) Training process of learning the optimal control policy for rocket powered landing: the control loss versus iteration; here we have performed five trials (labeled by different colors) with random initial guess of the policy parameter. (b) Validation: we use the learned policy to obtain the rocket control trajectory; here we also plot the ground-truth optimal control solved by an OC solver. The results in (a) and (b) show that the PDP can successfully find the optimal control policy (or optimal control sequence) to successfully perform the rocket powered landing. Please find the video demos at the link <https://youtu.be/5Jsu772Sqcg>.

The experiment process is similar to the experiments performed for the other three systems in Appendix E. We set the time horizon as $T = 50$, and randomly choose an initial state condition \mathbf{x}_0 for the rocket. We minimize the control loss function, which is now a given control objective function with θ_{obj} known. The control policy we use here is still parameterized as the Lagrangian polynomial, as described in (A.26) in Appendix E, here with degree $N = 25$. The learning rate is set to $\eta = 10^{-4}$, and we run five trials with random initial guess of the policy parameter. The the control loss $L(\xi_\theta, \theta)$ versus iteration is plotted in Appendix Fig. 15a. To validate the learned optimal control policy, we use it to obtain the control trajectory, and compare with the ground truth optimal trajectory obtained by an OC solver. The validation results are in Appendix Fig. 15b. Please find the video demos at the link <https://youtu.be/5Jsu772Sqcg>.